STUDY ON INSULATING PROPERTIES OF MINERAL OIL BASED ZnO NANOFLUID USING DIELECTRIC SPECTROSCOPY

A THESIS SUBMITTED IN PARTIAL FULFILLMENT FOR THE DEGREE OF MASTER OF TECHNOLOGY IN NANO SCIENCE AND TECHNOLOGY

By

SUSMITA GHOSH

CLASS ROLL NO.: **002130701027**

EXAMINATION ROLL NO.: **M4NST23010**

REGISTRATION NO.: **160448 OF 2021-2022**

Under the guidance of

Dr. ARPAN KUMAR PRADHAN

DEPARTMENT OF ELECTRICAL ENGINEERING

FACULTY OF ENGINEERING AND TECHNOLOGY

JADAVPUR UNIVERSITY

KOLKATA – 700032

2023

JADAVPUR UNIVERSITY

Kolkata – 700032, INDIA

FACULTY OF INTERDISCIPLINARY STUDIES, LAW AND MANAGEMENT

CERTIFICATE OF RECOMMENDATION

This is to certify that the thesis entitled "**Study on Insulating Properties of Mineral Oil Based ZnO Nanofluid Using Dielectric Spectroscopy**", is being submitted by **Ms. Susmita Ghosh (**Examination Roll No.M4NST23010), under our supervision and guidance during the session of 2021-22 in the School of Material Science and Nano Technology, Jadavpur University. We are satisfied with her work, which is being presented for the partial fulfilment of the degree of **Master of Technology in Nano Science and Technology** from Jadavpur University, Kolkata-700032.

Dr. Arpan Kumar Pradhan

Assistant Professor
Department of Electrical Engineering
Jadavpur University
Kolkata, 700032

Dr. Sourav Sarkar
Director
School of Material Science and Nano Technology
Jadavpur University
Kolkata, 700032

Prof. Tusher Jash
Dean
Faculty of Interdisciplinary Studies, Law and Management
Jadavpur University
Kolkata, 700032

JADAVPUR UNIVERSITY

KOLKATA – 700032, INDIA

FACULTY OF INTERDISCIPLINARY STUDIES, LAW AND MANAGEMENT

CERTIFICATE OF APPROVAL

The forgoing thesis entitled "**Study on Insulating Properties of Mineral Oil Based ZnO Nanofluid Using Dielectric Spectroscopy**" is hereby approved as a creditable study of an interdisciplinary subject carried out and presented in a manner that fulfills its acceptance as a prerequisite to the degree for which it is submitted. It is understood that by this approval, the undersigned does not necessarily endorse or approve any statement made, opinion expressed, or conclusion drawn there in but approves the thesis only for the purpose for which it is submitted.

The final examination for evaluation of the thesis

_____ _____

Signature of the Examiner (s) Signature of supervisor

DECLARATION OF ORIGINALITY AND COMPLIANCE OF ACADEMIC ETHICS

I hereby declare that the thesis contains literature survey and original research work by the undersigned candidate, as part of the Masters of Technology in Nano Science and Technology.

All the information in this document has been obtained and presented in accordance with academic rules and ethical conduct.

I also declare that, as required by these rules and conduct. I have fully cited and referenced all material and results that are not original to this work.

Name	:	**Susmita Ghosh**
Examination Roll no.	:	**M4NST23010**
Registration no.	:	**160448** of **2021-2022**
Thesis Title	:	**Study on Insulating Properties of Mineral oil Based ZnO Nanofluid Using Dielectric Spectroscopy**

Signature with Date:

ACKNOWLEDGMENTS

The Project work related, "**Study on the Insulating Properties of Mineral Oil Based ZnO Nanofluid Using Dielectric Spectroscopy**", was carried out at the High Tension Laboratory of Jadavpur University, Kolkata. I would like to take this opportunity to thank my teachers and well wishers for their cooperation and inspiration during the course of work

I express my sincere gratitude to my supervisor, Dr. Arpan Kumar Pradhan for his encouragement, suggestion, and advice, which made the thesis possible to be completed successful. I am very much grateful to Prof. Biswendu Chatterjee and Dr. Sovan Dalai for being a constant source of encouragement, and inspiration and for his valuable suggestions coupled with his technical expertise throughout my research work. It was a great honour for me to pursue my research under their supervision.

With great Pleasure, I would like to express my gratitudes to Dr.Sourav Sarkar and Dr.Chandan Kumar Ghosh for their keen interest and support in this work. I would like to render special thanks to Dr.Swarnendu Sen for guiding me consistently.

I would also like to thank my co-worker Mr. Biswajit Chakraborty, research scholar in High Voltage Engineering Department and the research scholars of Nanoscience and Technology department for providing constant encouragement throughout my thesis work.

Last but not least I extend my words of gratitude to my parents for personally motivating me to carry out the work smoothly.

ABSTRACT

This thesis basically proposes some advance methods to predict the time after the instant of preparation and the percentage concentration of nanofluids using dielectric spectroscopic methods. For this purpose, zinc oxide (ZnO) nanofluids based on mineral oil is prepared in the laboratory with different concentrations (i.e. 0.01%, 0.03%,0.05%, and 0.07%). First, ZnO nanoparticles are synthesized by low temperature hydrothermal method in laboratory. By employing X-ray diffraction methods, the average diameter of the ZnO nanoparticles is found to be 28.21nm. After that, ZnO nanofluids is prepared using two-Step process. To ensure the uniform dispersion of the nanoparticles, sonication followed by stirring process is employed. After the preparation of nanofluids, Polarization & Depolarization Current and Frequency Domain Spectroscopy measurement is conducted with different concentration along with several hours from the instant of sample preparation. From the time domain spectroscopy, various parameters are extracted using extended Debye model which are sensitive to the time after the instant of preparation and the percentage concentration of nanofluids. Similarly, from frequency domain spectroscopy, low frequency dispersion of capacitances and dielectric dissipation factor are evaluated which are found to be sensitive to the time after the instant of preparation and the percentage concentration of nanofluids. Using those aforementioned parameters, fourteen empirical relations are established. Then, to validate these relations, two samples are prepared in the laboratory with two different percentage concentrations of nanofluids. After that, the same experiments are conducted at two specific different instants from the time of preparation. Finally, percentage errors are calculated using those measured and obtained values. Based on this errors value, it can be stated that, using this method the time after the instant of preparation and the percentage concentration of nanofluids can be predicted accurately. This study further helps to prepare a long term stable nanofluids which may be used as a good alternative to mineral oil.

CONTENTS

List of Acronyms

Abbreviation	Full From
AC	Alternating Current
BVD	Breakdown Voltage
C_0	Geometrical Capacitance
C'	Real component of the complex capacitance
C''	Imaginary component of the complex capacitance
DC	Direct Current
FDS	Frequency Domain Spectroscopy
β	Full Width Half Maxima
I_{pol}	Polarization current
I_{depol}	Depolarization current
LFD	Low Frequency Dispersion
NF	Nanofluid
NPs	Nanoparticles
PDC	Polarization and Depolarization current
TDS	Time Domain Spectroscopy
$tan\delta$	Dielectric Dissipation Factor
σ_{ac}	AC Conductivity
XRD	X-ray Diffraction
θ	Bragg's angle.

List of Figures

List of Tables

CHAPTER- 1

INTRODUCTION

1.1 Introduction

Transformers are considered as an asset to the power system networks. Lifespan and condition of those transformers mainly rely on their insulating medium. Mineral oil serves this insulating purpose of those transformer and many high voltage equipment due to its superior dielectric properties. It also has good pouring point at low temperatures, good thermal cooling capacity, affordable price and its efficiency level is very high. It also serves as a cooling medium in those equipment [1-3]. However, today's increasing power demand raise the necessity for searching a new class of insulation which can provide improved dielectric properties. In this context, the concept of nanotechnology has been applied in the transformer oil for further enhancement of the dielectric properties of mineral oil. The concept of "nanofluid" was first introduced by Dr. Choi in 1995. Nanofluid (NF) is a newly discovered product of nanotechnology that used as a coolant and dielectric fluid. It is developed by uniformly dispersing the colloidal particles (diameter size is typically in the order of 1-100 nm) into conventional base fluids [5,6]. To ensure the long-term stability, additional substances like surfactants, dispersants are likely to be used during the preparation of nanofluids. The surfactants are incorporated into the nanofluids to prevent the agglomeration, caused by the nanoparticles due to its large surface to volume ratio (S/V). Dr. Choi [7] identified numerous advantages of the nanofluids over conventional liquid dielectrics which includes increased surface area, substantial heat flow rate, and stronger breakdown strength. There are mainly three types of nanoparticles (i.e. conducting, semiconducting and insulating) used with transformer oil. For enhancing the dielectric properties of transformer oil, enhancement of dielectric strength is the main criteria of the researchers. In this context, conducting nanoparticles are found to be more suitable than the semiconducting and insulating nanoparticles [9]. However, the main issue that creates obstacle for long term usage of nanofluids is their dispersion stability. To prepare the long term stable nanofluids, the concentration of the nanofluids and the time from the preparation are considered as important parameters those need to be optimized.

Form the past few decades, transformer oils have been successfully used as insulating and cooling materials due to their thermal as well as insulating properties. It has been reported in [1], improper dielectric insulation and poor design mainly responsible for the transformer's failures. Transformer is considered as the one of the most important electrical components as it has been potentially able to distribute electricity to the consumers [1]. It has been proven that transformers are a costly component and has an immediate impact on the manner in which the network operates, where it is located, how much oil is in it, and how much hazardous material

is present. Any disruption related to the transformer will decrease the reliability of the power system [2-4]. As per [5], overheating and thermal stress are considered as the major causes of transformer failure. Hence, to overcome transformers failure caused by the aforesaid factors, many researches and approaches have been introduced. For this purpose, various nanoparticles mainly (conducting, semiconducting and insulating) have been dispersed in the mineral oil to enhance both thermal and dielectric characteristics. The homogeneous dispersion of nanoparticles in the base fluid are known as nanofluids. Due to its exceptional dielectric qualities, it attracted a lot of attention by the researchers [6-7]. Moreover, Still, researchers are trying to find the best possible combination of nanoparticles and mineral oil (nanofluids) to have improved characteristics [7].

In the years between the 1870s and the 1990s, petroleum-based oils have been employed in the transformer system to provide necessary insulation [6]. Apart from this, it also serves as a cooling medium in that equipment. Due to their high paraffin wax concentration, paraffinic-based oils generally have high pour points, which is undesirable for use in power-distribution equipment subjected to low temperatures. From [8], it has been reported that, high-viscosity oils have a lower ability to transport heat, which in turn results in overheating and a shorter shelf life. Whereas, transformer oil based on naphthenic has been developed to overcome the aforementioned obstacles. Despite the fact that oils with a naphthenic base are more susceptible to oxidation than paraffinic based oil because the oxidised products from paraffinic-based materials are soluble, viscosity was reduced [7]. Oils with naphthenic bases have a lower pour point and will stay liquid in the transformer system at low temperatures.

Therefore, the concept of nanotechnology has been applied in the transformer oil for enhancement of the dielectric properties of mineral oil. Now to increase the heat dissipation of insulation oil, Siginer et al. first suggested an insulation oil-based nanofluid in 1995 [3]. It has been reported in [4], due to the incorporation of nano-aluminum nitride (nano-AlN) with 0.5 vol% in mineral oils can effectively increase thermal conductivity by up to 8%. Also, from [5-11], it has been found that, addition of aluminium oxide (Al_2O_3), Silicon dioxide (SiO_2), silicon carbide (SiC), hexagonal boron nitride (h-BN), graphene, and others in the mineral oil can effectively increase the insulating characteristics. Comparison with the unmodified mineral oil, Segal et al. discovered in 2000 that positive lightning impulse breakdown voltage (BDV) of mineral oil based nanofluids increased by up to 50% [12-14]. Although dispersion of nanoparticles into the mineral oil are advantageous, but due to the large surface to volume ratio (S/V) of nanoparticles, there is a tendency of agglomeration or sedimentation in the nanofluids.

Hence to ensure the long-term stability, additional substances like surfactants, dispersants are likely to be used during the preparation of nanofluids [13].

Therefore, based on the aforesaid observations, it has been clearly indicated that, incorporation of nanoparticles into the base oil have been effectively used to replace the conventional dielectric fluids in the transformers Although nanofluids are capable to enhance both electrical and thermal qualities but it must be able to withstand against of thermal, electrical stresses etc. Moreover, regular monitoring of the transformer insulation condition is very necessary to prevent early failure of the transformer. The investigation has been conducted in the time and frequency domains. The polarization & depolarization current (PDC), recovery voltage measurement (RVM) are considered as very effective techniques in the time-domain measurement. Whereas, frequency domain spectroscopy (FDS) is very effective technique in frequency domain for determination of the dielectric properties. It should be stated here that, FDS is advantageous than time domain [15-17].

In this work, conducting zinc oxide (ZnO) nanoparticles with a mean diameter of 28.21nm were dispersed in the mineral oil that acts the base oil of the nanofluids with different volume fractions (i.e. 0.01%, 0.03%,0.05%, and 0.07%). Then, the prepared ZnO nanofluids were subjected to PDC and FDS measurement. These measurements were carried out considering several hours from the instant of preparation or with different percentage concentration of the nanofluids. Hence, from FDS and PDC measurements, some parameters have been extracted through which hours from the instant of preparation or percentage concentration of the nanofluids can be predicted.

1.2 The Motivation for the Work

With the recent advancement in the field of nanotechnology, nanofluids are widely being preferred in the power system industry due to its large surface area and ability for the enhancement of breakdown strength. Hence, a comprehensive study has been done in this thesis work, for the enhancement of insulation capabilities of the mineral oil by applying the concept of nanotechnology. Here in that experiment, condition assessment of the transformer insulation has been carried out through dielectric spectroscopic measurements in both the time and frequency domains. Moreover, from the dielectric spectroscopic measurements, various parameters have been extracted through which hours from the instant of preparation or percentage concentration of the laboratory prepared ZnO nanofluids can be predicted.

Therefore, the aim of this thesis work is to monitor how these parameters are sensitive to the hours from the instant of preparation and percentage concentration of the nanofluids.

1.3 Outline of The Thesis

The thesis is organized as follows:

- Chapter 1 introduces the preliminary idea of the thesis work. It includes my motivation for the work.
- Chapter 2 consists of the existing previous works related to this work.
- Chapter 3 consists of detailed information regarding transformer insulation and application of nanotechnology in transformer oil.
- Chapter 4 provides information regarding the synthesis of nanoparticles and steps to prepare nanofluids. Thereafter, different dielectric properties of nanofluids were discussed in details.
- Chapter 5 provides the brief theory about time and frequency domain spectroscopic measurement.
- Chapter 6 consists of the preparation and characterization of ZnO nanoparticles involving necessary steps. Further, an experimental set-up was developed to conduct time and frequency domain spectroscopic measurement.
- Results obtained from X-ray diffraction method, dielectric spectroscopy in time and frequency domain were discussed in chapter 7. From these results, few parameters were extracted from PDC and FDS. Using these parameters, hours from the instant of preparation and percentage concentration have been predicted.
- Chapter 8 discuss the conclusions of this work and state few challenges which needs to be explored in future.

CHAPTER-2

OVERVIEW OF TRANSFORMER INSULATION: ADVANCEMENT WITH NANOTECHNOLOGY

2.1 Transformer Insulation

The control and functioning of the power transformer play a key role in the power system's stability. Transformers are essential parts of electricity transmission and distribution networks because they increase or decrease the voltage levels, which facilitates effective energy transfer. Transformer insulation is very essential in power systems because transformers operates at voltages between thousands and millions of volts, which is a high voltage.

Insulation materials, such as insulating oils, paper, or synthetic materials, are used to avoid electrical breakdown and ensure the safe and reliable operation of the transformer. The strength of the insulation, quick cooling techniques, and regular inspection are the three most crucial components that ensure a transformer will run steadily [18]. It has been seen that insulation materials that have high dielectric strength are capable of withstanding high voltage without allowing electric current to pass through them. In order to achieve this, transformers use insulating oil which offers the necessary thermal stability, electrical insulation, and arc-prevention in the event of a fault. These characteristics could be satisfied by a variety of oil that is widely available on the market [19–21]. Among them mineral oil is used as liquid insulation in the majority of transformers due to its extensive dielectric properties and resistance. Due to its superior electrical insulating qualities. it can successfully prevent electrical failures and maintain the necessary insulation resistance. This property is essential for transformers, as they operate at high voltages.

Hence, it can be concluded that transformer insulation is essential for the mechanical, electrical, and thermal safety of power systems. It guarantees reliable and safe operation, guards against electrical failure, regulates voltage levels, dissipates heat, protects against environmental factors, and supports the transformer mechanically.

2.2 Mineral oil as Transformer oil

In order to manufacture mineral oil, which is a non-renewable fossil resource, crude oil distillate needs to first go through extra physical and chemical processing under atmospheric pressure before being processed again under vacuum. The mineral oil has three fundamental chemical compositions, they are paraffinic, naphthenic and aromatic. Mineral oil was originally used as transformer oil in 1892 by General Electricals after Eliu Thompson obtained a patent for it that was chemically stable [22]. Since then, it has experienced several changes, including changing from its naphthenic to paraffinic form and also in the manufacturing process, and is still utilised as an insulating liquid in the power industry. The structures of the naphthenic,

paraffinic, and aromatic hydrocarbons—which are essentially the building blocks of refined mineral oil are shown in Fig. 3.1. Mineral oil can be used to accomplish the characteristics of a good insulating oil, including high dielectric strength, high temperature stability, and low dielectric loss [23].

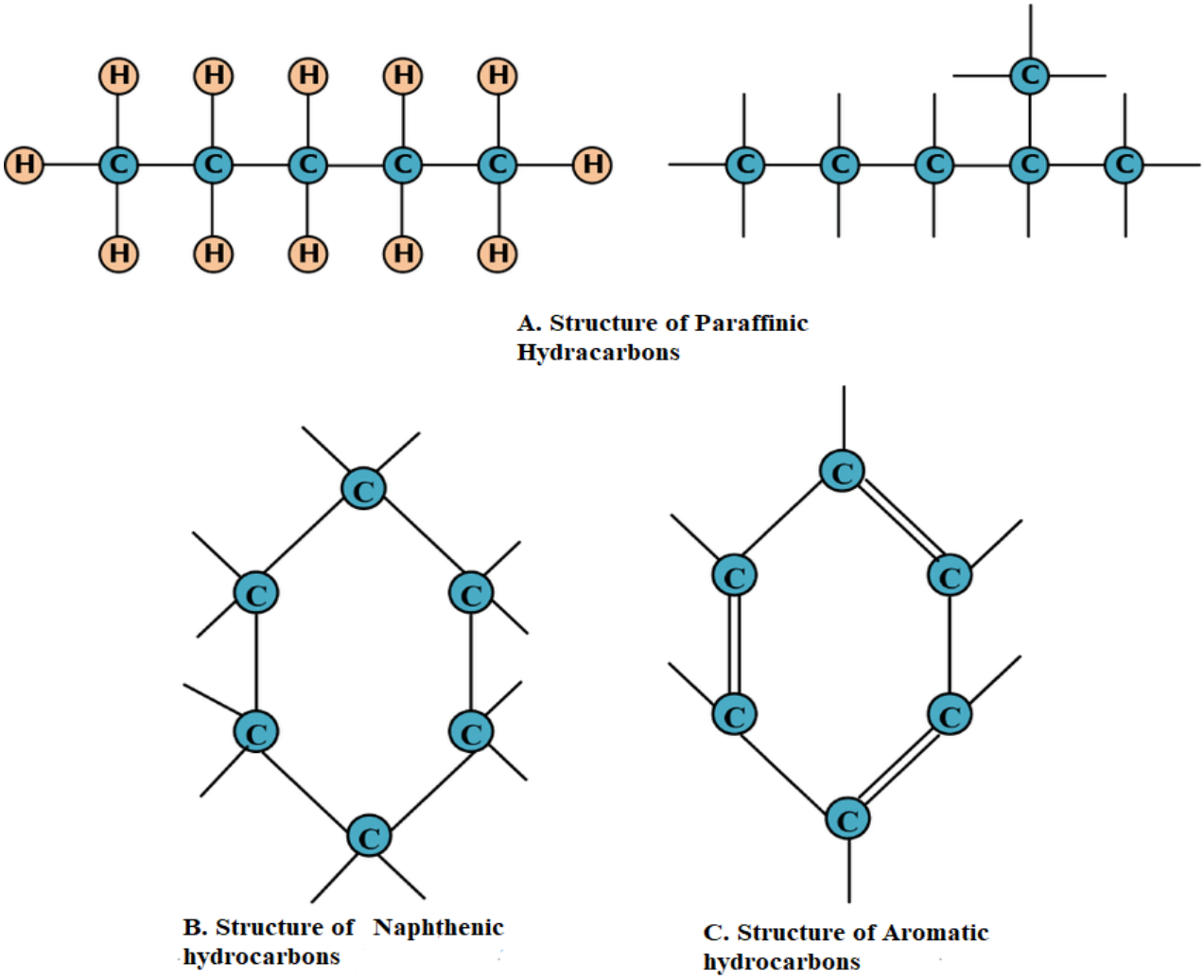

Fig. 2.1. Basic carbon structures in mineral oil molecules [22]

Additionally, there are two main categories for mineral oil are paraffinic and naphthenic. Both naphthenic oil and paraffinic oil have lower proportions of naphthene hydrocarbons and paraffinic hydrocarbons, respectively [23]. The two types of mineral oil both have benefits as well as drawbacks. When used as intended, naphthenic oil has a shorter lifespan than paraffinic oil because it becomes oxidized more quickly [24]. In terms of sludge generation, naphthenic oil surpasses paraffinic oil [25]. When it comes to removing the sludge content, paraffinic oil

performs less well than naphthenic oil. The specifications of the two types of oils have been given in Table.2.1.

Table 2.1. Specifications of the two types of oils [24]

Property	Naphthenic Oil	Paraffinic Oil
At 20℃ Density in kg/m^3	882.9	872.8
Kinematic viscosity at 20℃ in mm^2/s	9.655	10.06
Pour point (℃)	-45	-24
Flash point (℃)	140	159
Acidity in mg KOH/g	0.01	0.022
Breakdown voltage for electrodes with a 2.5mm gap (kV)	55	42
Nature of sulphur	Non- corrosive	Non-corrosive

2.3 Study of Nanofluids

It has been reported in [9], Feynman introduced the idea of nanotechnology in 1959. That has been used in several scientific disciplines, most notably physics, engineering, material science, etc. Using nanotechnology, it is become possible to manipulate the matter at the nanoscale (roughly in the range of 1-100nm) which efficiently improve the materials' various characteristics. The same idea holds true for nanofluids, which are dielectric liquids that possess nanoparticles incorporated to improve their thermal and dielectric properties. The term “nanofluid” was first introduced by Dr. Choi and Eastman in 1995.The nanofluids are the base fluids that have nanoscale particles uniformly floating throughout them. As per [26,27], In accordance to many researches, adding nanoparticles into transformer oil will raise the breakdown voltage. Researchers are still looking for a perfect combination of nanoparticles and transformer oil (nanofluids) to have superior characteristics. In addition to having significant effects on the thermal properties of composite materials, the volume fraction of nanoparticles, surface to volume ratio (S/V), their shape and size, and the surface contact area between particles and liquid are important parameters. The study of mineral oil based nanofluids has recently attracted a lot of interest [28]. Numerous nanofluids for use in power transformers have drawn attention for their dielectric and thermal properties. As reported in [29–30], thermal conductivity and AC and DC breakdown voltages are better in magnetic nanofluids than in unmodified mineral oil.

A fluid that contains nanosized particles is often referred to as a nanofluid. Manufactured colloidal suspensions of nanoparticles in a base fluid make up these fluids [31,32]. The nanoparticles in nanofluids are typically made of metals, oxides, carbides, or carbon nanotubes. There are two phases in these systems: a solid phase and a liquid phase. Nanofluids have been found to have better thermal conductivity, thermal diffusivity, viscosity, and convective heat transfer coefficients than base fluids like oil or water. It has demonstrated a diverse range of potential applications. A two-phase system has a number of critical issues that need to be resolved. One of the most significant problems is the stability of nanofluids, and it is still very difficult to achieve the proper stability of nanofluids. This chapter gives an overview of the stability mechanism and recent advancements in stable nanofluid production methods. Nanofluids have gotten increased attention in recent years. Applications for a wide spectrum of nanofluids are primarily influencing research in this area. Although some review articles on the advancement of nanofluid research have been published recently [33-35], the majority of the reviews are focused on theoretical and experimental investigations of the thermophysical characteristics or convective heat transfer of nanofluids. Thus, in addition to describing the heat transfer properties of nanofluids, this chapter will concentrate on the new methods for preparation and stability mechanisms. Recent advancements in stable nanofluid preparation methods will be discussed in the following sections along with an overview of the stability processes.

2.3.1 Types of Nanoparticles

Nanoparticles can be roughly categorised into a number of groups based on their morphology, size, and chemical characteristics. The choice of nanoparticles for the fabrication of nanofluids must be made with extreme care; typically, permittivity and conductivity are used as the primary criterion for selection. Therefore, one should first analyzed all the properties of the material, which will help in increasing the dielectric strength of the fluid. The nanoparticles are broadly classified into three main categories, conductive (includes ferric oxide (Fe_3O_4) and zinc oxide (ZnO)), semi conductive (includes titanium dioxide (TiO_2), copper oxide (CuO_2)) and insulating (includes boron nitride (BN) and silicon oxide (SiO_2)), respectively.

Apart from the aforementioned categories, the nanoparticles can be classified into the following groups,

- **Carbon Based Nanoparticles**:

The two primary components of carbon-based NPs are fullerene and carbon nanotubes (CNTs). Single-walled carbon nanotubes (SWCNTs) and multi-walled carbon nanotubes (MWCNTs) are two different types of CNTs. Among them, fullerene is an allotrope of carbon with a hollow cage structure made up of sixty carbon atoms or more. The structure of C-60 is similar to a hollow football. Due to their excellent electrical conductivity, extraordinary strength, and electron affinity make them suitable for numerous applications.

- **Ceramic Nanoparticles:**

Ceramic NPs are an inorganic solid which made from phosphates, carbides, oxides, and carbonates. These NPs have excellent chemical internes and heat resistance.

- **Polymer Nanoparticles:**

Organic-based NPs are polymer NPs. Depending on the production method, they have configurations that resemble nanocapsules or nanospheres. Despite having a core-shell structure, nanosphere particles are arranged in a matrix-like manner**.**

- **Lipid Based Nanoparticles:**

The majority of lipid nanoparticles (NPs) have spherical shapes with diameters between 10 and 100 nm. It consists of a matrix made up of soluble lipophilic molecules and a solid lipid core. For these types of nanoparticles, emulsifiers and surfactants are used to stabilise the outer core of these NPs.

2.3.2 Dielectric Properties

The dielectric characteristics of nanofluids will unavoidably alter significantly as a result of the addition of nanoparticles [40-41]. In mineral insulating oil, Sartoratto et al. introduced surface-modified Fe_3O_4 magnetic nanoparticles [42]. The results demonstrate that the addition of nanoparticles significantly enhanced the electrical resistivity, imaginary part of the dielectric constant and dielectric loss factor and the relative permittivity stays constant until the volume proportion of nanoparticles reaches 0.016. The dielectric loss factor of nanofluids is 0.1868, which is 51 times greater than that of pure oil (0.0036), when the volume percentage of nano-Fe_3O_4 is 0.8%. Additionally, magnetic nanoparticles decrease volume resistivity, making them potentially harmful when used in the electrical field for applications involving nanofluids. Merges et al. investigated the effect of frequency on the dielectric properties of nano-oil, and

they reported that in the frequency range of 0.1 Hz to 10^6 Hz, Fe_3O_4 based nanofluids showed higher relative permittivity, and in the frequency range of 0.1Hz to 10^6 Hz, dielectric loss factor is also increased [43]. Du et al. looked at how temperature affected the dielectric characteristics of nanofluids. In various oil temperature ranges, conductive Fe_3O_4 nanoparticles have reduced electrical resistivity and raised the dissipation factor. However, insulated BN nanoparticles had a good dielectric characteristic that enhanced electrical resistance and decreased dissipation factor [44]. Li et al. looked into the dielectric characteristics of a Fe_3O_4 nanofluid made from vegetable oil [40, 45]. When the frequency is below 10 Hz, they discovered that the dielectric loss factor of nano-oil is significantly lower than that of pure oil, and when the frequency is above 100 Hz, they discovered that the volume resistivity of nanofluids is higher than that of pure vegetable oil. The majority of studies were AC BDV-centric, and there haven't been many investigations into DC BDV or positive impulse voltage. The mineral oil-based nanofluid a Fe_3O_4 (diameter of a Fe_3O_4 nanoparticle is around 10 nm; practically spherical) is at the top of the list with the largest improvement in AC and DC BDV and positive impulse voltage. The positive impulse BDV and conductivity of nanofluids with rod-like TiO_2 nanoparticles increased 23 and 60.7%, respectively, in comparison to that of TiO_2 nanospheres, according to Lv et al.'s study of the morphology, which includes the size and shape of nanoparticles that affects their dielectric properties [46].

2.3.3 Thermal Properties

The potential of nanofluids in heat transfer applications has drawn increasing attention, since the concept of nanofluids was first proposed by Dr.choi in 1995. As of now, a few review papers [47-53] have been published that provide overviews of many aspects of nanofluids, such as preparation and characterization, methods for measuring thermal conductivity, theory and model, thermophysical characteristics, and convective heat transfer. The thermal conductivities of ethylene glycol (EG)-based nanofluids containing oxides like MgO, TiO_2, ZnO, Al_2O_3 and SnO_2 nanoparticles [54], the MgO-EG nanofluid was found to have superior characteristics, having the highest thermal conductivity and lowest viscosity.

2.3.4 Stability of Nanofluids

In addition to settling and blockage of microchannels, the agglomeration of nanoparticles lowers the thermal conductivity of nanofluids. As a result, stability research is an important aspect that affects the application-relevant characteristics of nanofluids, and it is important to research and evaluate the factors that affect the stability of nanofluid dispersion. This section

will contain the Stability mechanisms of nanofluids. The dielectric and insulating properties of the nano-insulating oil will be impacted if the nanoparticles agglomerate because of the surface energy and interface energy and are no longer stable. Van der Waals force, electrostatic force, solvation power, gravity, buoyancy, and other forces will all be applied to the nanoparticles when they are disseminated in the base fluid [55], and the stability of their dispersion is directly correlated with both their physical and chemical characteristics. According to the DVLO theory, the van der Waals attractive forces and electrical double layer repulsive forces jointly control the stability of nanofluids [56, 57]. It implies that the nanofluid will be stable if the repulsive forces are greater than the attractive forces. It will be possible to see aggregation brought on by collisions or sedimentation brought on by gravity with nanoparticles that lack or have a very low concentration of surfactant. However, the double chain surrounding the surface of the nanoparticles will create an extra steric repulsive force when there is an excess of surfactant, as illustrated in Fig.4.3., thirdly, the DVLO hypothesis states that electrostatic stabilization is another technique to increase the repellent forces for nanoparticles. These factors prevent the aggregation of nanoparticles and guarantee the stability of nanofluids.

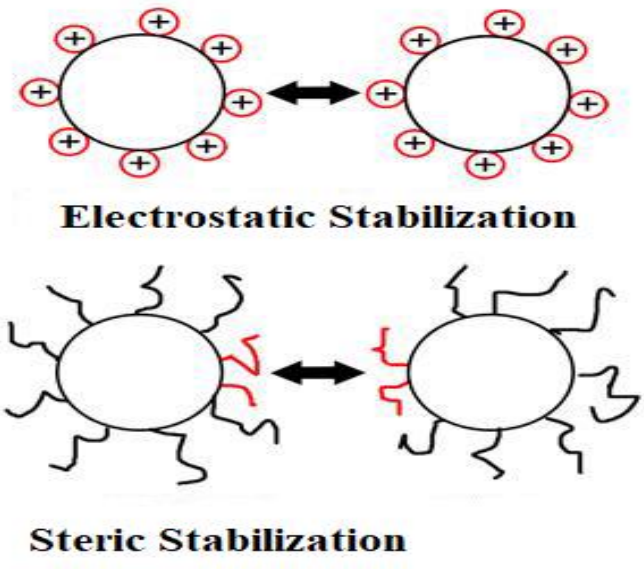

Fig.2.2. Concept of steric and electrostatic stabilization [55]

4.7 Advantages & Disadvantages of Nanofluids

Form the aforementioned sections, it can be concluded that the addition of nanoparticles in the base fluids can effectively increases some properties. The nanofluids includes the following advantages,

- The dispersed nanoparticles enhance the fluid's effective thermal conductivity.
- The enhanced specific surface area of the particles increases the interaction between the base fluid and the nanoparticles.

But, due to the large surface area of the nanoparticles, there is a tendency for agglomeration or sedimentation of the particles in the base fluids. Apart from this, the processing expenses of the nanofluids are very high. Also, rapid clustering is a big issue when dealing with the nanofluids.

CHAPTER-3

THEORITICAL BACKGROUND ON X-RAY DIFFRACTION AND DIELECTRIC SPECTROSCOPIC MEASUREMENT

3.1. Theory of X-ray Diffraction Method

X- ray diffraction method is an important technique for determining the structure of the crystals. The theory behind XRD is a result of pioneering works of the Braggs.

Bragg's law suggests that the crystal structures can be considered as an array of atoms/molecules that forming planes.

The X-ray incident on an atom will scatter in some direction. The scattered X-rays can interfere constructively if they are in-phase or destructively if they are out of phase.

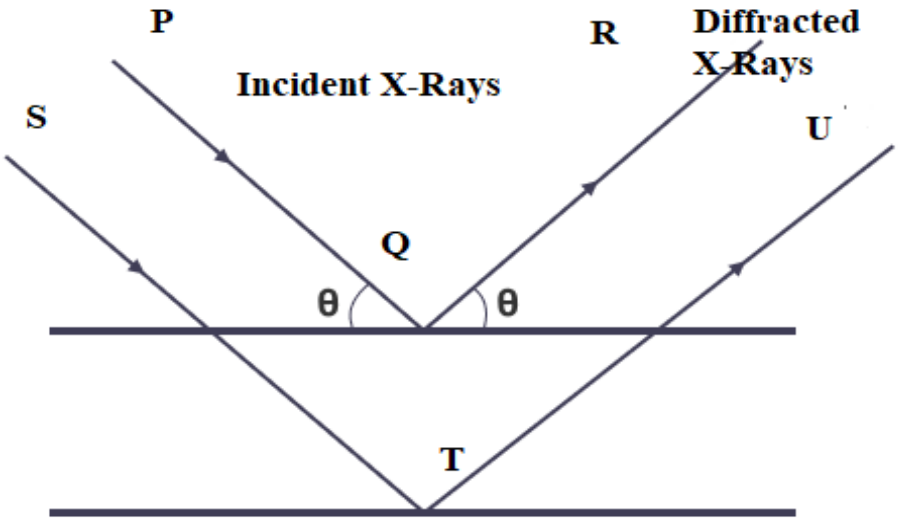

Fig.3.1. Concept of Bragg's Law

The path difference between the two x-rays scattering from the two planes can be seen to 2dsinθ, where *d* is the interplanar distance and θ is the incident angle.

For the two waves to interfere constructively, they should satisfy, the following relation

$$2d\sin\theta = n\lambda \qquad (3.1)$$

According to Bragg's law, the relation between interplanar distance (*d*) and wavelength of x-ray (λ=*0.15406 nm*) has been represented in (3.1) and n is considered as order of peak selected.

Now if the XRD graph for a crystalline material is considered, some intense peaks can be found. But for an amorphous material no such peaks will be found. Now using JCPDS card, the material can be easily identified and then by using Scherrer formula, the mean size of the material can be determined from the XRD graphs as given in (3.2) [60].

$$D = \frac{k\lambda}{\beta \cos\theta} \tag{3.2}$$

Where, *D* represents the crystalline Size of the nanoparticle, *k* represents Scherrer constant (for spherical structure, it is 0.9) and β is the line broadening at half of the maximum intensity (full width half maxima).

3.2 Dielectric Response Method

In order to prevent transformer failure, insulation should be regularly monitored before its time of operation. For this purpose, dielectric response analysis has been developed to evaluate the insulation state of transformers. The two basic categories of this investigation are conducted in the time and frequency domain. For these purposes, polarization & depolarization current (PDC) is an effective technique that is used in time-domain spectroscopy measurement. Whereas, frequency domain spectroscopy (FDS) is effectively used in frequency domain for determination of insulation capabilities. Hence, a brief theory related to PDC and FDS has been discussed in the following section.

3.2.1 Concept of Time Domain Spectroscopy

The polarization process starts when an electric field is applied across a dielectric. The inner dipoles are directed in the direction of the applied electric field as a result of the polarization process. Conduction current and displacement current start to rise as a result of the effects of polarisation [58,59]. Hence, electric displacement can be defined as,

$$D(t) = \varepsilon_0 \varepsilon_r E(t) + \Delta P(t) \tag{3.3}$$

In this case, the permittivity in free space, relative permittivity of the dielectric material, applied electric field and the polarization function are denoted as $\varepsilon_0, \varepsilon_r$, E(t) and P(t), respectively. P(t) is the dielectric response function that has a monotonically decaying characteristics can be written as (3.4).

$$P(t) = \varepsilon_0(\varepsilon_\infty - 1)E(t) + \varepsilon_0 \int_0^t f(t-\tau)E(\tau)d\tau \tag{3.4}$$

ε_∞ is the relative permittivity of the material at high frequencies. In (3.4), the first term represents rapid polarization, and the second term represents slow polarization. Ampere's law can be used to calculate the current density through a dielectric material in an electric field E(t). Therefore,

$$J(t) = \sigma E + \varepsilon_0 \frac{\partial}{\partial t}\{\varepsilon_\infty E(t) + \int_0^t f(t-\tau)E(\tau)d\tau\} \quad (3.5)$$

In (3.5), the first term represents conduction current, and the second term represents polarization current. The current passing through the test object can therefore be expressed as follows, assuming that external voltage U(t) that generates the electric field E(t). Hence the current, due to the effect of DC conductivity, permittivity and dielectric response function can be written as (3.6).

$$I(t) = C_0 \left(\frac{\varepsilon_0}{\sigma_0} + \varepsilon_\infty \delta(t) + f(t)\right) U(t) \quad (3.6)$$

In (3.6), C_0 is referred as the geometrical capacitance of the test sample.

The time domain dielectric diagnosis mainly includes Polarization and depolarization current method. This technique records charging and discharging currents of the insulation. The measurement of polarization and depolarization currents (PDC) following a dc voltage step is one way in the time domain to investigate the slow polarization processes. The dielectric memory of the test object must be cleared before the PDC measurement. The voltage source should be free of any ripple and noise in order to record the small polarization current with sufficient accuracy.

The schematic of the PDC measurement has been given in the Fig.3.2.

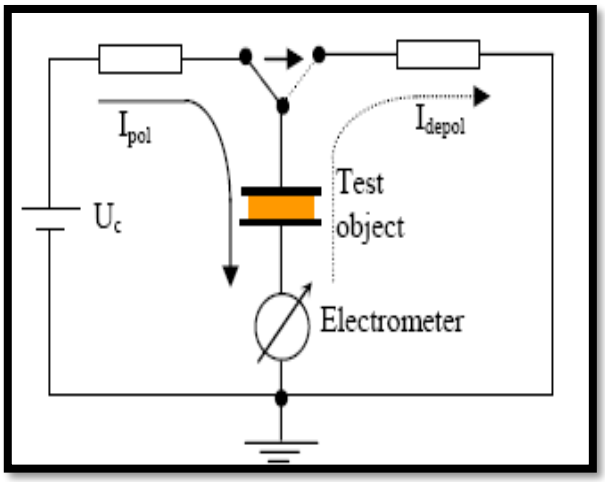

Fig.3.2.PDC measuring Circuit [59]

The procedure consists in applying a dc charging voltage of magnitude U_c to the test object for a long time (For e.g. 10,000s). During this time, the polarization current $I_{pol}(t)$ through the test object is measured, arising from the activation of the polarization process with different time

constants corresponding to different insulation materials and to the conductivity of the object, which has been previously carefully discharged.

In the following section, the typical characteristics of the polarization and depolarization current have been shown in Fig.3.3.

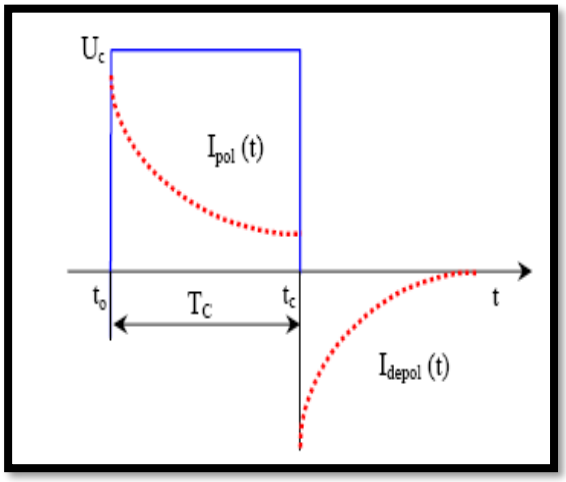

Fig.3.3. Typical nature of polarization and depolarization current [59]

From Fig.3.3, the typical nature of polarization and depolarization current has been studied. The insulation between windings is charged by the dc voltage step Uc. From Fig.3.3, it has been concluded that, the initial time dependence of the polarization and depolarization currents (<100 s) is very sensitive to the conductivity of the mineral oil.

Now the value of dc conductivity can be obtained from the aforementioned PDC curves (Fig.3.3) by subtracting the depolarization current from the polarization current at larger values of time. Therefore, the dc conductivity σ_0 can be expressed by (3.7).

$$\sigma_0 = \frac{\varepsilon_0}{C_0 V_{dc}} [i_{pol}(t) - i_{depol}(t)] \tag{3.7}$$

3.2.1.1 Background theory on Extended Debye Model

From time domain spectroscopy measurements, a model has been developed to create an equivalent circuit through which insulation characteristics can be effectively studied. The several R- C branches that make up this model has been shown in Fig. 3.4. The internal dipoles of a dielectric material begin to line up with the direction of the applied electric field. Polarization current flows as a result of this orientation. The dielectric shorts out when an

applied electric field is withdrawn after a specified amount of time. The dipoles start to realign themselves to their initial locations, releasing the bound charges on the electrodes. Therefore, if the external circuit is complete over a meter, these free charges flow as discharging or depolarization current. Every dipole group has a unique polarization current and relaxation time. Each dipole group is represented by a unique R-C branch in an electric field in the extended Debye model.

The dc conductivity in polarization current is represented by the R_0 term in the extended Debye model. In the extended Debye model, the delta function in polarization current is represented as C. Every R-C branch of the extended Debye model can be shown in Fig.3.4. as an active polarization process.

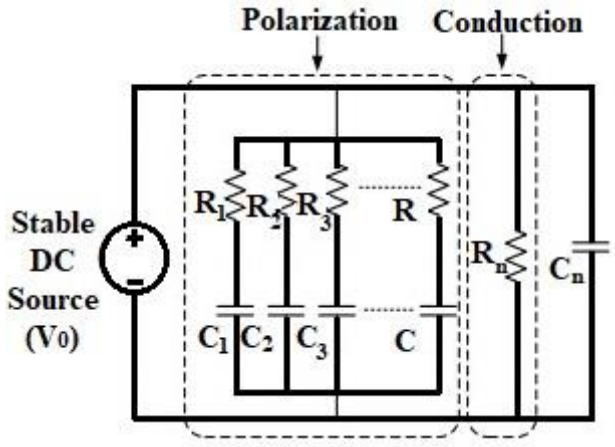

Fig. 3.4. Equivalent circuit of the extended Debye model [59].

The conduction current and current due to the dipolar polarization makes the polarization current. Whereas, due to the impact of dipole reorientation, the depolarization current developed.

Hence, polarization current can be written as,

$$i_{pol} = i_c + i_{d(pol)} \tag{3.8}$$

($i_{d\,(depol)}$) as defined by (3.9).

$$I_{depol} = I_{d\,(depol)} \tag{3.9}$$

(I_{depol}) can be written as (3.10)

$$i_{d\,epol} = -\sum_{k=1}^{n} A_{(k)} \times (e^{-\frac{t}{\tau}})\; i_{d\,epol} = -\sum_{k=1}^{n} A_{(k)} \times (e^{-\frac{t}{\tau}}) \tag{3.10}$$

where, τ_k is the time constant for active polarization process, and A_k is the decaying coefficient as defined by (3.11).

$$A_k = \frac{U_0}{R_k}[1 - e^{\frac{t_c}{\tau_k}}] \tag{3.11}$$

$$\tau_k = R_k C_k \tag{3.12}$$

The value of R_0 of the extended Debye model can be calculated by using (7.8).

$$R_0 = \frac{U_0}{I_{pol(t_c)} - I_{depol(t_c)}} \tag{3.13}$$

where, U_0 is the applied electric field across an insulation dielectric.

The branch parameters of the extended Debye model can be effectively calculated using (3.11), (3.12) and (3.13).

3.2.1.2 Advantages of PDC Method

- This non-destructive method can provide the moisture content in the solid insulation material and the conductivities of the oil and paper.
- Other diagnostic quantities like activation energy and polarization spectra can be calculated from PDC measurements directly.
- It provides very fast response at low frequencies with good accuracy.

3.2.2 Frequency Domain Spectroscopy

Dielectric response in the frequency domain is another alternative method to study the polarization phenomena. This is an ac test and, dissipation factor or tan delta is measured as a function of frequency of test. The frequency range for FDS is normally between 1 m Hz to 1 kHz. This involves measurement of impedance at different frequencies and possibly at different voltages also. The dielectric is energized with sinusoidal voltages and the current across it is measured. Measurements in the frequency domain need voltage sources of variable frequencies and, for applications related to HV power equipment, output voltages up to at least some hundreds of volts. The impedance is then calculated which helps in the evaluation of power factor, capacitance, dissipation factor, permittivity etc. Here in this section, Fig. 3.5 shows the basic FDS measurement circuit.

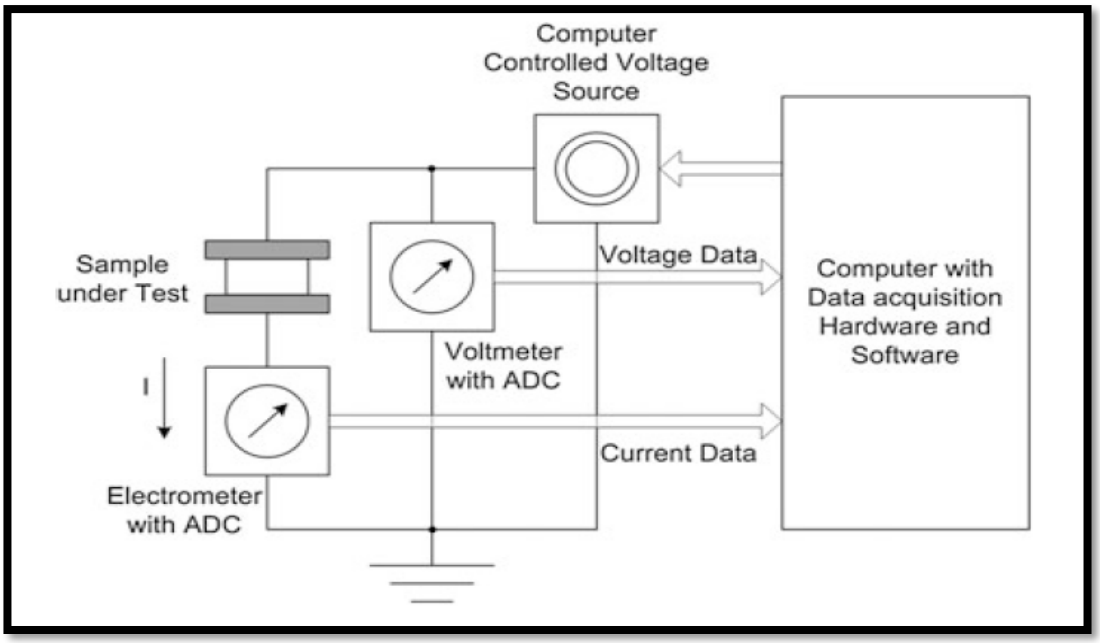

Fig. 3.5. FDS Measurement Circuit [14]

When an alternating field is introduced, the dipoles in the dielectric material start to align with the electric field. The insulating material's free electrons begin to move in the direction of the anode as well. The alignment of the dipoles and the flow of the electrons towards the anode influence the electric current that travels from anode to cathode through the dielectric material. The effect of electron mobility and dipole alignment on each other affects the nature of current. According to [14], the current's quality seems to deteriorate over time. As a result, the time domain current can be analytically transformed to the frequency domain by employing the Laplace transform or Fourier transform.

Therefore, with an application of pure sinusoidal excitation, the current flowing through the dielectric material can be characterised in the frequency domain by,

$$\overline{I(\omega)} = j\omega\, \overline{C(\omega)}\overline{U(\omega)} \tag{3.14}$$

Where, current through the dielectric material is represented by $\overline{I_\omega}$ and the equivalent complex capacitance of the dielectric material is resented by $\overline{C(\omega)}$ .The expression of $\overline{C(\omega)}$ is given in (3.15).

$$\overline{C(\omega)} = C'(\omega) - jC''(\omega) \tag{3.15}$$

In (3.15), $C'(\omega)$ is the real component of the complex capacitance, which in general denotes the capacity to store energy due to dipoles and electrons. Whereas, $C''(\omega)$ is the imaginary component of complex capacitance, which often represents energy loss during dipole alignment and electron transport. The dipoles interact with the molecules or other existing

dipoles when alignment takes place in a dielectric medium under an alternating field. The frictional loss produced by these contacts raises a dielectric loss [15]. The electron is driven towards the anode when an electric field is introduced. As a result, any molecules, electrons, or dipoles that are already present are hit by travelling electrons. By generating energy loss within the dielectric material, this collision increases the dielectric loss. Generally, the imaginary component of the complex capacitance, $C''(\omega)$ indicated this dielectric loss. In (3.16), $C'(\omega)$ basically represents the energy storage capability that takes place in the dielectric material as a result of the electrons' transporting to the anode and the dipoles' alignment with the applied field. The $tan\delta$ is a parameter that can be used to estimate the state of an insulating material [16]. It is the ratio between the imaginary component of the complex capacitance, which indicates energy loss, and the energy storage component, or the real part of the complex capacitance, is known as the $tan\delta$. The expression of $tan\delta$ is given in (3.16).

$$tan\delta = \frac{C''(\omega)}{C'(\omega)} \tag{3.16}$$

According to [14], electron transport in an insulating material under an electric field and the alignment of the dipoles are extremely slow processes that are effective in the power frequency range (i.e.50 Hz) and below it. In order to acquire a clear image, frequency domain spectroscopy (FDS) is used at very low frequency ranges, from 1 mHz to 1 kHz or more [8, 10].

3.2.2.1 Theory on Low Frequency Dispersion

From frequency domain spectroscopy, nature of various parameters such as $tan\delta$, C' and C'' at low frequency range (i.e. from 1mHz to 100Hz) can be easily analyzed. Moreover, it has been observed that the peak in the dielectric loss factor occurs at low frequencies and reaches its minimum at high frequencies. Another fact can be observed at low frequencies, when charge carries near the electrode surface reduces due to the effect of space charge polarization Due this reduction of charge carriers, the capacitances are significantly increasing but as a consequence, ac conductivity decreases. Therefore, a study of low frequency dispersion features of the real and imaginary components of the capacitance or tanδ has been realized to investigate insulation characteristics.

For this purpose, the change in real and imaginary components of complex capacitance or $tan\delta$ are obtained from the following equations (3.17), (3.18), (3.19).

$$\Delta C' = C'_{1mHz} - C'_{100Hz} \quad (3.17)$$

Where, C'_{1mHz} and C'_{100Hz} are the real component of complex capacitance obtained at 1 mHz and 100 Hz.

$$\Delta C'' = C''_{1mHz} - C''_{100\ Hz} \quad (3.18)$$

Similarly, C''_{1mHz} and C''_{100Hz} are the imaginary component of complex capacitance obtained at 1 mHz and 100 Hz, respectively.

$$\Delta tan\delta = tan\delta_{1mHz} - tan\delta_{100Hz} \quad (3.19)$$

Where, $tan\delta_{1mHz}$ and $tan\delta_{100Hz}$ are the tanδ values obtained at 1 mHz and 100 Hz frequency.

From FDS, the value of ac conductivity can be easily determined by (3.20).

$$\sigma = \frac{C'' \times \varepsilon_0 \omega}{C_0} \quad (3.20)$$

Where, σ is the ac conductivity, C″ is imaginary capacitance, ε_0 is permittivity in free space (8.854×10^{-12} F/m) and C_0 is considered as the geometrical capacitance of the test cell. From equation (3.20) the relationship between ac conductivity and imaginary capacitance can be established.

3.2.2.2 Advantages of FDS Method

- Dielectric frequency domain spectroscopy (FDS) enables measurements of the composite insulation capacitance, permittivity, conductivity (and resistivity) and loss factor in dependence of frequency.
- The real and imaginary components of the complex capacitance and permittivity can be separated.
- This non-destructive technique also provides the moisture content in the solid insulation material and C-ratio diagnostic quantity.
- FDS has better noise performance and separates the behavior of polarizability (χ') and losses (χ'') of a dielectric medium.

CHAPTER-4

EXPERIMENTAL SETUP AND PROCEDURE

4.1 Selection of Material for Sample Preparation

For investigation of the insulation properties of nanofluids an experimental set-up has been developed in the laboratory. For this purpose, mineral oil (MO) has been selected as the base oil for the nanofluid sample. In the fabrication of a nanofluid sample, conductive ZnO nanoparticles have been selected with a mean diameter of approximately 28.21 nanometres. In the selection of the nanoparticles, conductivity and permittivity are the two fundamental parameters that must be considered. Here, an electrode made up of two 30.48 cm x 30.48 cm aluminium sheets spaced apart by 4 mm is used; the structure of this electrode is shown in Fig. 4.1. After that, the electrode is dipped into the prepared nanofluid sample with full precautions. Using the experimental setup depicted in Fig.4.5. both time and frequency domain spectroscopy measurements have been conducted on mineral oil based ZnO nanofluid sample.

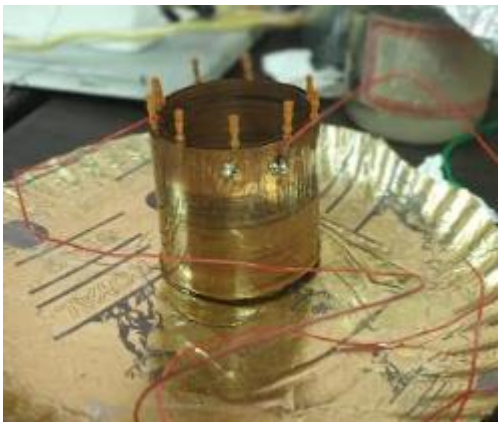

Fig. 4.1. Electrode set up

4.2 Sample Preparation

In this section, the synthesis process of ZnO nanoparticles have been discussed. After that, the preparation method of the mineral oil based ZnO nanofluids have also been discussed.

4.2.1 Synthesis process of ZnO Nanoparticles

In this section, the method for preparation of zinc oxide nanoparticles has been discussed. Here, for the synthesis of zinc oxide nanoparticles low temperature hydrothermal process has been applied. For the manufacture of zinc oxide nanoparticles, pentahydrate salts of zinc nitrate [Zn $(NO_3)_2.5H_2O$] and hydroxide salt of sodium (NaOH) have been chosen as precursors. In a typical low-temperature hydrothermal synthesis of ZnO nanostructures, 0.47 gm of [Zn $(NO_3)_2$, $5H_2O$] was dispersed in 25 ml of deionized (DI) water before 15 ml of NaOH solution was incorporated dropwise and vigorously stirred at ambient temperature for approximately 5 minutes. After that, the mixture was put into a 250 ml Scott bottle and heated hydrothermally

up to 100 ° C. Precipitates were collected after 5 hours of reaction by centrifugation at 3000 rpm for 18minutes, and then they were dried for 2 hours at 60 ° C.

The instrument set up used for the preparation of ZnO nanoparticles by low temperature hydro thermal process have been shown in Fig.4.2.

Fig.4.2. Experimental set up for low temperature hydrothermal method.

After that, phase purity and crystallinity of the synthesized ZnO nanoparticles were analyzed using the X-ray diffractometer (specification: CuKα radiation, λ=1.5404 Å, Ultima III, Rigaku, Japan) which have been given in Fig.4.4. This method was adopted to examine the structure and morphology of the laboratory prepared ZnO nanoparticles [60].

4.2.2 Preparation of Mineral Oil Based Nanofluid

Here, mineral oil based ZnO nanofluids have been prepared by two step method. For fabrication of nanofluid sample, conductive ZnO nanoparticles have been selected with a mean diameter of approximately 28.21 nanometres. The entire process is classified into three steps, as follows:

- For preparation of mineral oil based nanofluids, 22 mg of Zinc Oxide nanoparticles were dispersed in the mineral oil with four different volume fractions (0.01%,0.03%,0.05% and 0.05%). For this purpose, 400 ml of mineral oil was taken in

the beaker into which ZnO nanoparticles were added at four different percentage concentration.

- After that, dispersion of the nanofluid was carried out by using a magnetic stirrer for around 30 minutes in order to get uniform dispersion.
- To ensure homogeneous dispersion of the nanofluid, it was applied to ultrasonication for 99 minutes. In order to lower the content of dissolved water in the prepared nanofluid sample, it was carried out in a vacuum oven for at least 1 hour.

Fig.4.3. shows the procedures needed to prepare a sample of ZnO nanofluid based on mineral oil.

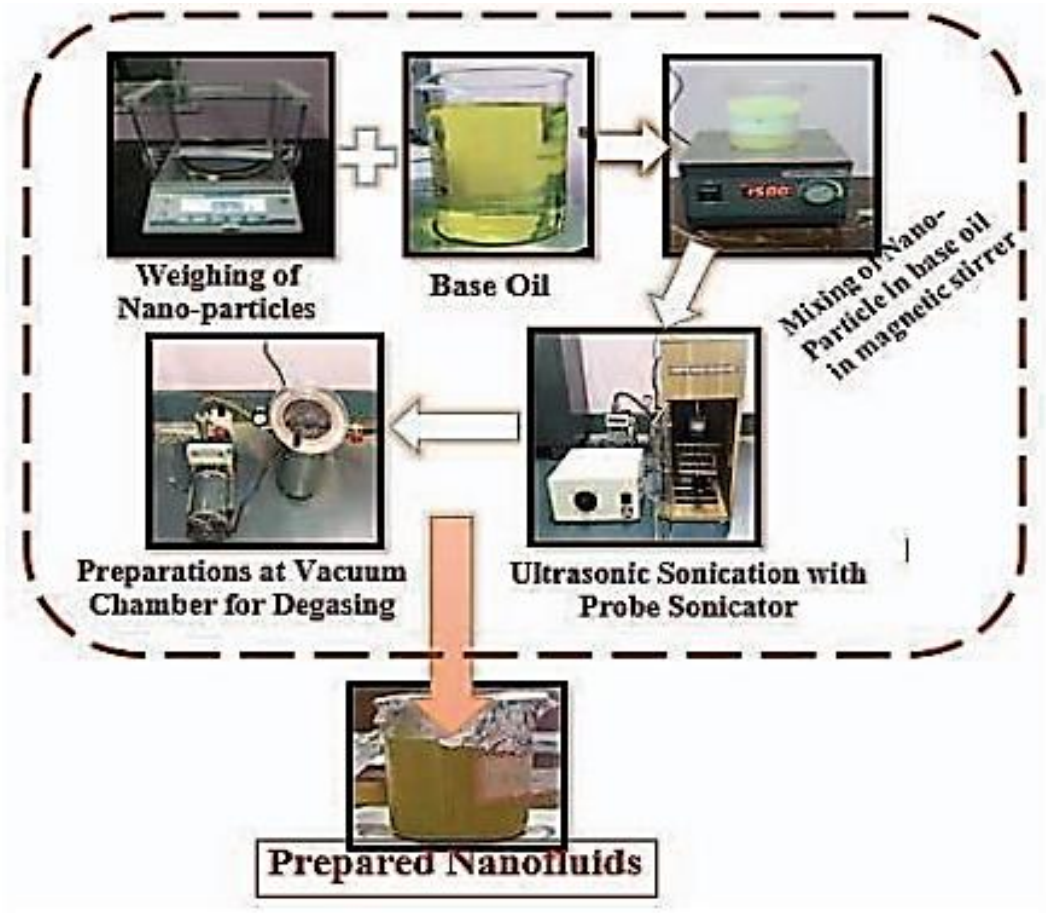

Fig. 4.3. Steps for Preparation of Nanofluids [39]

4.3 Experimental Process

In this section, characterization of laboratory prepared ZnO nanoparticles have been discussed by employing X-ray diffractometer instrument. After that, experimental procedures for investigation of the insulating properties of nanofluid samples have been discussed in both time

and frequency domains. In this context, Fig.4.6. illustrates the experimental setup for both PDC and FDS measurements.

4.3.1 Characterization of laboratory prepared ZnO nanofluids by X-ray diffraction method.

A simple X- ray diffractometer instrument requires a radiation source, sample crystal and a detector. The instrument set up used for the characterization of laboratory prepared ZnO nanoparticles has been shown in Fig.4.4. This characterization method has been performed for structural and morphological analysis of the laboratory prepared nanoparticles.

Fig.4.4. X-Ray diffractometer Instrument

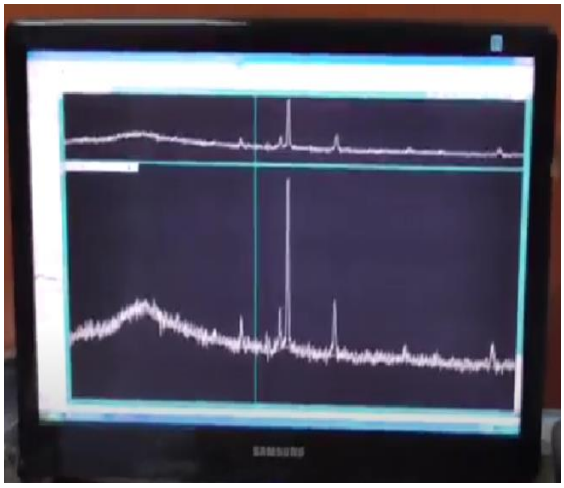

Fig.4.5. Data acquisition system

A source gives of x-rays that strike the crystal at some angle θ and the detector detects the scattered radiation at angle of 2 θ from the source. The x-ray hits the atoms in the crystal plane and scatter in different direction. For diffraction to occur, the scatter radiation must be coherent there for the scattering must be elastic. Thereafter, the intensities of the scattered radiation are recorded and plot interplanar distance versus 2θ. This is the plot of intensity of the scattered radiation vs 2θ. This plot of intensity is called XRD pattern. For this purpose, the intensity of the highest peak is set to 100 and rest of the peaks are called respect to this. Thus, the peaks are mapped to a particular set of lattice planes gives by the corresponding miler indices.

This is done by calculation of interplanar spacing corresponding to a particular peak and using relationship between d and the h,k,l indices for different lattice types.

In the following sections, the steps have been discussed through which XRD pattern has been derived.

- First, XRD pattern between the two data (intensity and the angle of diffraction). has been drawn using origin software.
- After getting the first plot, analysis has been done by using option “Smooth” under “Signal Processing”.
- Once the graph become smooth, next step is to analyse the peaks.
- After analyse the peaks, it is needed to correct the baseline of the pattern in order to get good quality image.
- In order to make the curve converge, it is needed to select all the peaks and open the option “Nlift”.in the origin software.
- Once it reaches the convergence, the software will show the analysis data of the graph including the θ and FWHM value.
- Now to calculate the crystalline size of the nanoparticles by Scherrer equation, the FWHM value should be converted into radians.

Therefore, by putting the values which are obtained from the XRD in (3.2) the crystalline size of the nanoparticles can be calculated approximately.

4.3.2 Time Domain Spectroscopy on Prepared Sample

For investigation of the insulation capability of laboratory prepared mineral oil based nanofluid sample, in time domain has been conducted employing DIRANA^{TM} at 25 °C and 100V. From time domain spectroscopy measurement, polarization and depolarization currents have been recorded for 1000 seconds of each sample (with percentage concentration and several hours).

6.3.2 Frequency Domain Spectroscopy on Prepared Sample

The insulation characteristics of the laboratory-prepared mineral oil-based ZnO nanofluid samples were investigated through conducting frequency domain spectroscopy (FDS) measurements employing DIRANA^{TM} for the prepared samples at various percentage concentrations of nanofluids, respectively. In that analysis, the voltage magnitude of the FDS measurement was fixed at 40Vrms. The experimental set-up for both PDC and FDS measurements has been shown in Fig.4.6.

Fig.4.6. Experimental set up for PDC and FDS measurements

CHAPTER-5

RESULTS AND DISCUSSIONS

5.1 Introduction

In this section, the structure and morphology analysis of the laboratory prepared zinc oxide (ZnO) nanoparticles have been conducted utilizing X-ray diffraction (XRD) method. Next, the interplanar distance between the atoms and crystalline size of the prepared zinc oxide nanoparticles have been determined.

After that, the results from the instant and frequency domain spectroscopy have been presented and analyzed with varying nanoparticles' volume fractions and time scales. Hence, from the instant domain results, the insulation has been modelled using extended Debye model. Then, from the model parameters empirical relationships have been established with nanoparticles' volume fraction or hours from the instant of preparation. Therefore, few parameters have been extracted from the frequency domain responses of a mineral oil-based ZnO nanofluid which can efficiently predict volume fractions of nanoparticles on hours from the instant of preparation. Moreover, Low Frequency Dispersion of C', C'' and $tan\delta$ have been determined which are also illustrated in this section. Finally, several empirical equations have been established between the LFD of C', C'' and $tan\delta$ with the nanoparticles volume fraction or hours from the instant of preparation.

5.2 Structural and morphological analysis of ZnO nanoparticles using XRD method

From XRD, a pattern has been determined using value of intensity and angle of diffraction (2θ) which identified at 2θ=31.7°, 34.4°, 36.2°, 47.5°, 56.5°, 62.8°, 67.7°and 68.8°. From the value of 2θ, it can be observed that, there are no other peaks which is not corresponds to ZnO. This fact in turn confirms of phase purity of the synthesized nanoparticle samples. The XRD patter of the laboratory prepared ZnO nanoparticles has been depicted in Fig.5.2a.

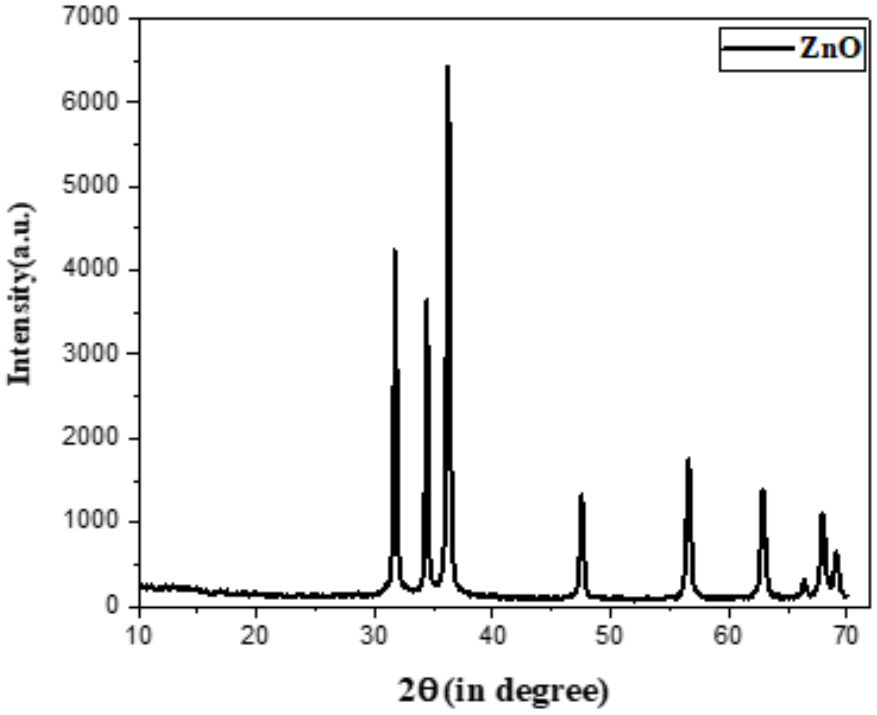

Fig. 5.2a. XRD pattern of ZnO

5.2.1 Determination of interplanar distance between the atoms

In this section, the interplanar distance between the atoms has been calculated using Bragg's law. For this purpose, five most intense peaks should be chosen. The data obtained from XRD has been given in Table 5.1.

Table 5. 1.

Results from XRD method

Intensity (a.u)	2θ (degree)	Θ (degree)	sinθ (degree)	n	nλ (nm)
4236	31.7	15.85	0.27312	218	33.58508
3595	31.8	15.9	0.27395	219	33.73914
3642	34.4	17.2	0.29570	245	37.74470
6424	36.2	18.1	0.31067	263	40.51778
5456	36.3	18.15	0.31150	264	40.67184

The interplanar distance between the atoms of the selected peaks have been calculated using (3.1) and given in Table 5.2.

Table 5. 2. Calculation of interplanar distance between the atoms

θ (degree)	Sinθ (degree)	n	nλ (nm)	d (nm)
15.85	0.27312	218	33.58508	61.484
15.9	0.27395	219	33.73914	61.5790
17.2	0.29570	245	37.74470	63.822
18.1	0.31067	263	40.51778	65.201
18.15	0.31150	264	40.67184	62.283

Hence, average value of interplanar distance between the atoms has been found as 62.87562 nm.

5.2.2 Determination of size of the crystalline zinc oxide

For the calculation of crystalline size of ZnO nanoparticles, Scherrer equation (given in (3.2)) has been used. From XRD pattern (Fig.5.2a.) and Table 7.1 value of 2θ corresponds to most intense peak is 36.2 ° and corresponding FWHM (β) value is obtained from origin software as 0.29627° or 0.00517 rad. Hence, using (3.2), crystalline size of prepared zine oxide nanoparticles can be calculated and found to be 28.21 nm.

5.3 Analysis of the results obtained from dielectric spectroscopy

In this section, dielectric response measurements in both time and frequency domain have been discussed. At first, time domain responses of mineral oil based ZnO nanofluids with different concentration and durations are analyzed. In the next part of this section, using extended Debye model, insulation of the mineral oil based ZnO nanofluid sample has been modelled properly. The prescribed model of time domain response is given in section 5.3.1.5. The validity of empirical equations connecting the model parameters with concentrations or hours from the instant of preparation has been covered in section 5.3.1.5.8.

Therefore, frequency domain responses of laboratory prepared nanofluids at different volume fraction of nanoparticles on different duration are analyzed. In the later part, the low frequency dispersion characteristics of C', C'' and $tan\delta$ with variation of hours from the instant of preparation or percentage concentration are illustrated. From the LFD study, some parameters are obtained through the nonlinear regression method for which the regression coefficient (R^2) is greater than 90% which point to good fitting, as presented in sections 5.3.3.1–5.3.3.5. After that, empirical relations have been established between the LFD of C', C'' and $tan\delta$ with the nanoparticles volume fraction or hours from the instant of preparation.

5.3.1 Dielectric Response in Time Domain

For investigation of the insulation capability of the laboratory prepared nanofluids, time domain spectroscopy (TDS) has been conducted employing DIRANA™ at ambient temperature (25 °C) and 100V. From TDS, polarization and depolarization currents have been recorded for 1000 seconds of each sample (with concentration variation and several hours).

5.3.1.1 Variation of polarization current with several hours.

Polarization current of different prepared samples has been plotted with several hours from the instant of preparation with four fixed concentration (0.01%, 0.03%, 0.05% and 0.07%), as shown in Fig. 5.3.1.1a - Fig. 5.3.1.1d. From Fig. 5.3.1.1a- Fig. 5.3.1.1d, it can be observed that, the polarization current steadily decreases with increasing hours from the instant of sample preparation.

Another interesting fact that can be observed from the aforementioned figures is that the conduction current is steadily decreasing from 24 hours to 48 hours for each sample. But from 72 hours to 96 hours, the conduction current for each sample becomes almost the same.

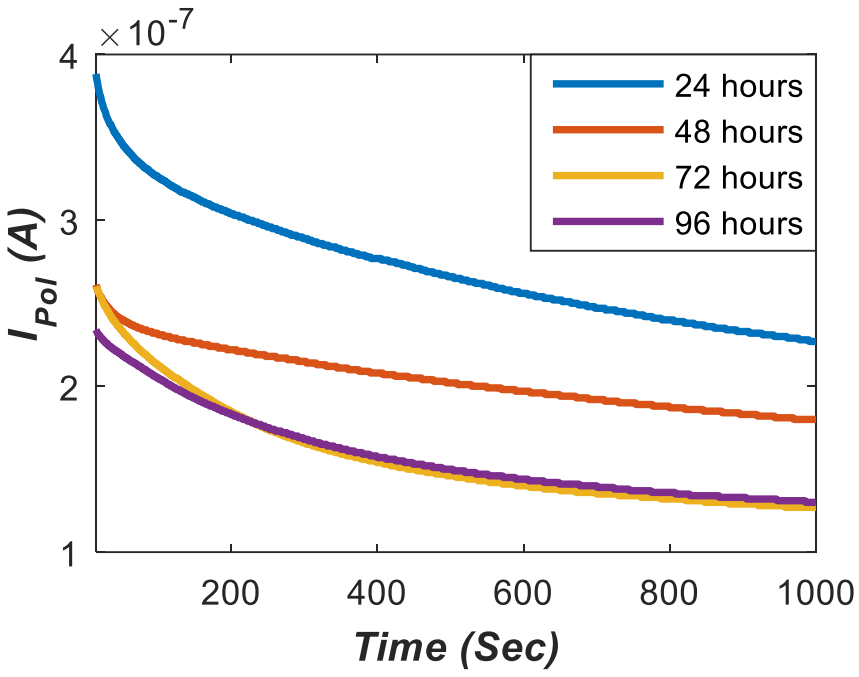

Fig. 5.3.1.1a. Variation of I_{Pol} at 0.01% volume fraction of ZnO nanofluids

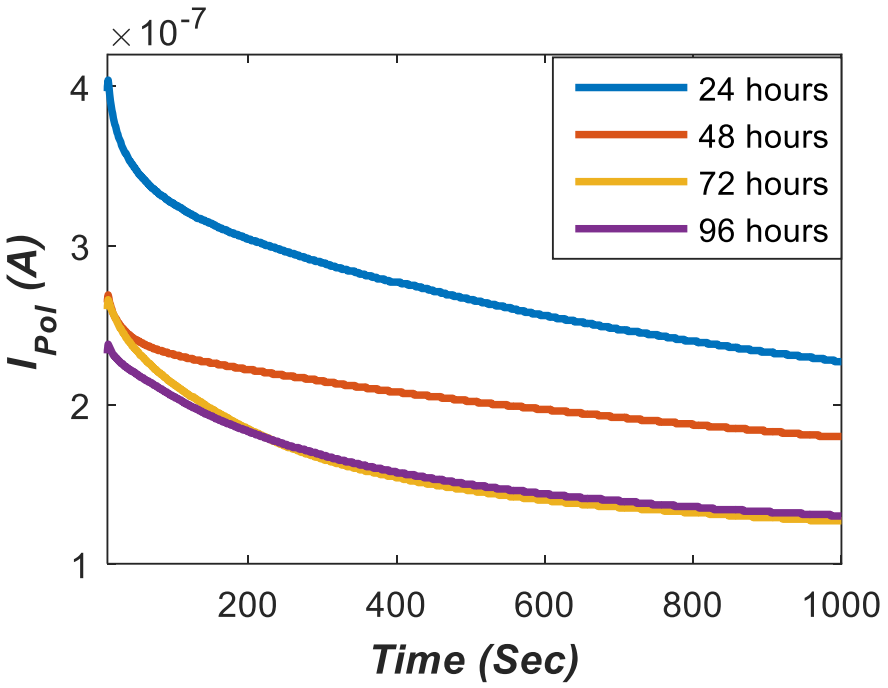

Fig. 5.3.1.1b. Variation of I_{Pol} at 0.03% volume fraction of ZnO nanofluids

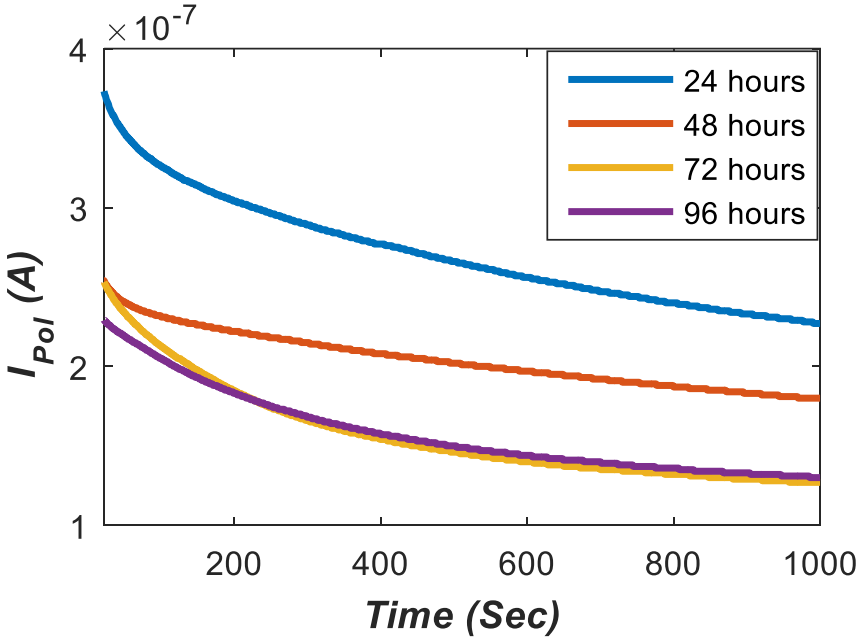

Fig. 5.3.1.1c. Variation of I_{Pol} at 0.05% volume fraction of ZnO nanofluids

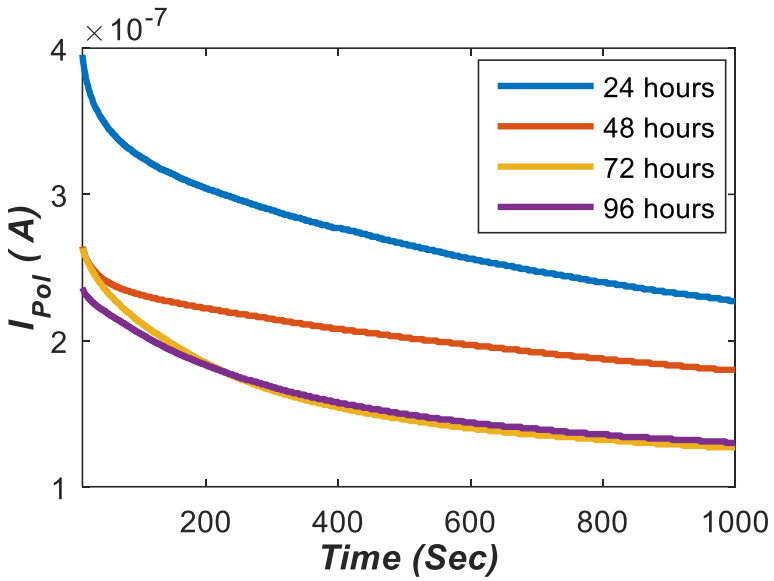

Fig. 5.3.1.1d. Variation of I_{Pol} at 0.07% volume fraction of ZnO nanofluids

5.3.1.2 Variation of polarization current with different percentage concentration.

The polarization current of laboratory prepared samples has been plotted with various percentage concentration with four fixed hours from the instant of preparation as shown in Fig. 5.3.1.2a. -5.3.1.2d.

From Fig.5.3.1.2a – 5.3.1.2d, it can be observed that the higher magnitude of the polarization current occurs at lower concentrations than at higher concentrations, which is a usual property of an insulating material.

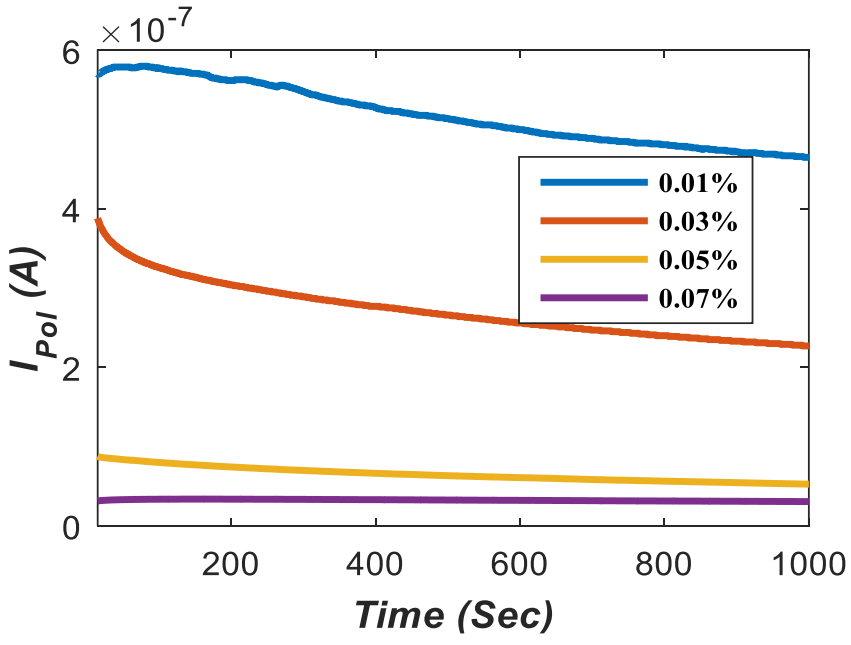

Fig. 5.3.1.2a. Variation of I_{Pol} at 24 hours by varying concentration

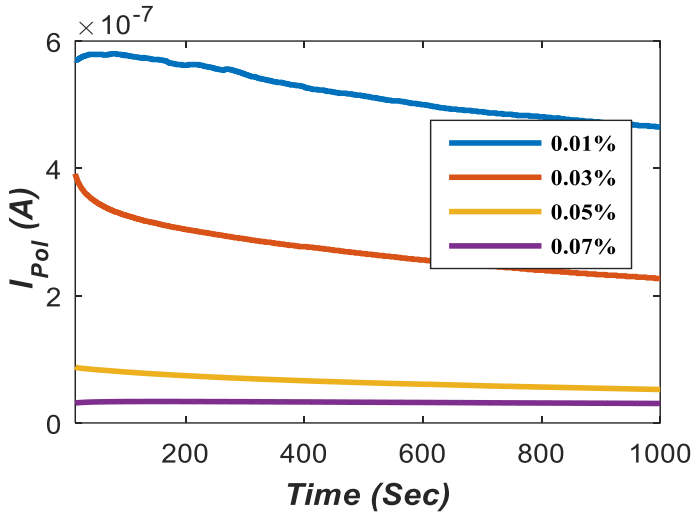

Fig. 5.3.1.2b. Variation of I_{Pol} at 48 hours by varying concentration

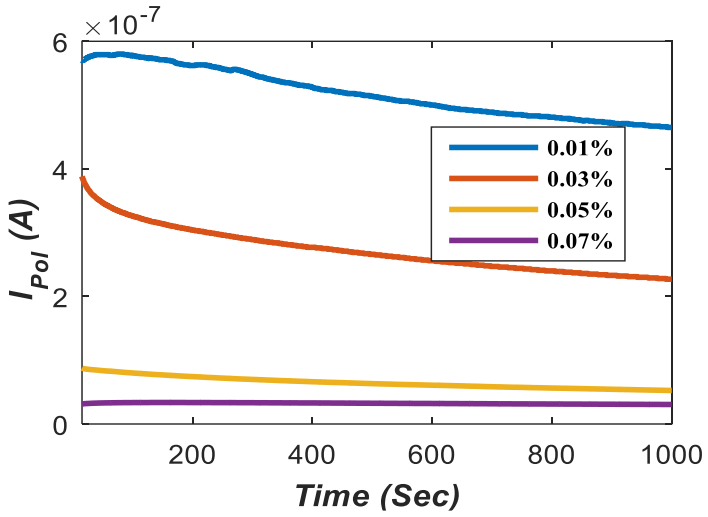

Fig. 5.3.1.2c. Variation of I_{Pol} at 72 hours by varying concentration

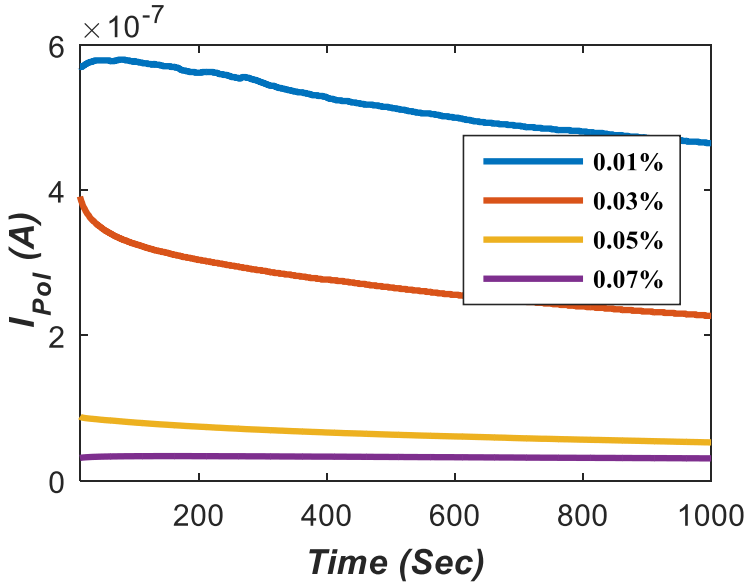

Figure 5.3.1.2d. Variation of I_{Pol} at 96 hours by varying concentration

5.3.1.3 Variation of depolarization current with several hours.

The depolarization current of different prepared samples has been plotted with several hours from the instant of preparation with four fixed concentration (0.01%, 0.03%, 0.05% and 0.07%), as shown in Fig. 5.3.1.3a - Fig. 5.3.1.3d.

From Fig. 5.3.1.3a, it can be illustrated that the depolarization current is higher for 24 hours from the instant of preparation and becomes almost the same from 72 hours to 96 hours.

Fig. 5.3.1.3b-Fig.5.3.1.3d, it can be observed that, the depolarization current steadily decreases with increasing hours from the instant of sample preparation.

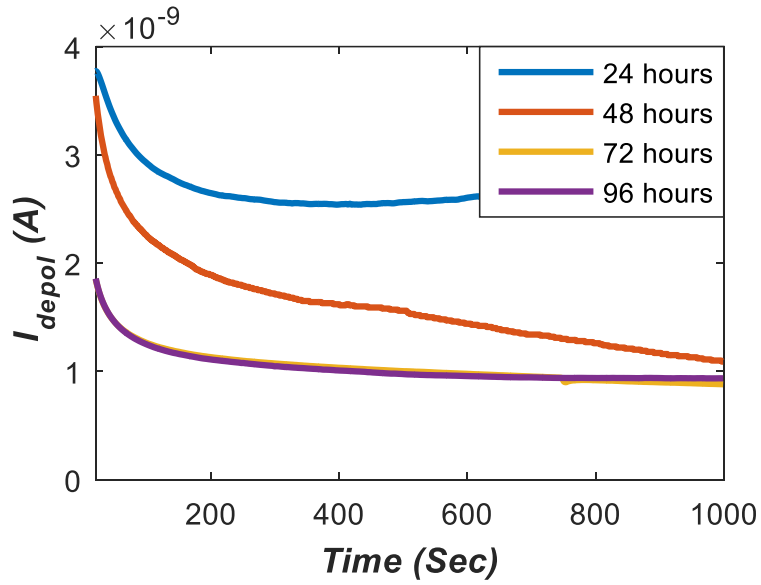

Fig. 5.3.1.3a. Variation of I_{dePol} at 0.01% volume fraction of ZnO nanofluids

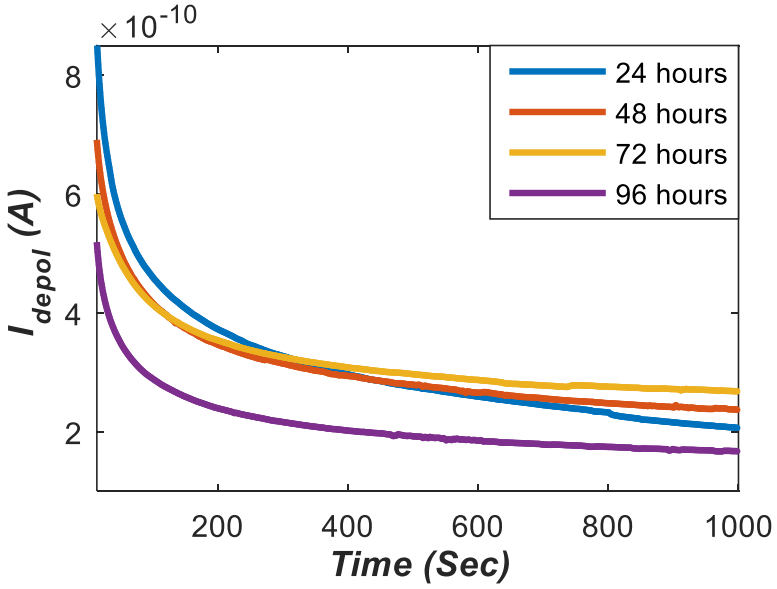

Fig.5.3.1.3b. Variation of I_{dePol} at 0.03% volume fraction of ZnO nanofluids

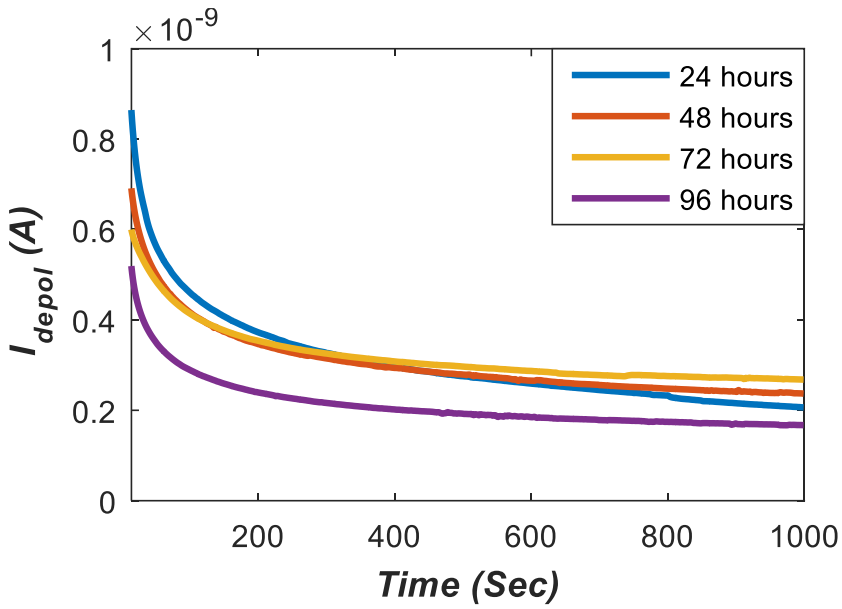

Fig.5.3.1.3c. Variation of I_{dePol} at 0.05% volume fraction of ZnO nanofluids

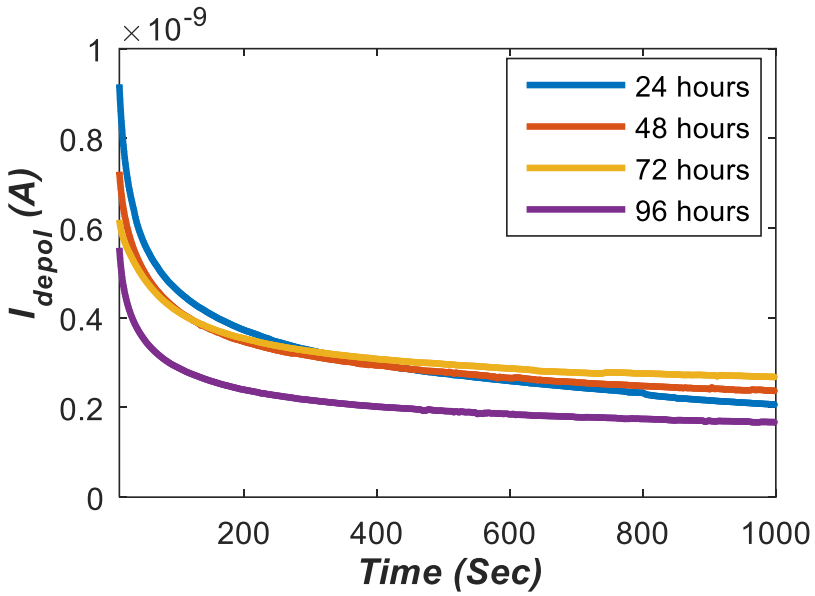

Fig. 5.3.1.3d. Variation of I_{dePol} at 0.07% volume fraction of ZnO nanofluids

5.3.1.4 Variation of depolarization current with different percentage concentration.

Here, the depolarization current of laboratory prepared samples has been plotted with various concentrations of nanofluids with four fixed hours from the instant of preparation as shown in Fig.5.3.1.4a-Fig.5.3.1.4d.

From Fig. 5.3.1.4a -Fig.5.3.1.4d it can be observed that, depolarization current is steadily decreasing with increasing the concentrations of laboratory prepared ZnO nanofluid samples.

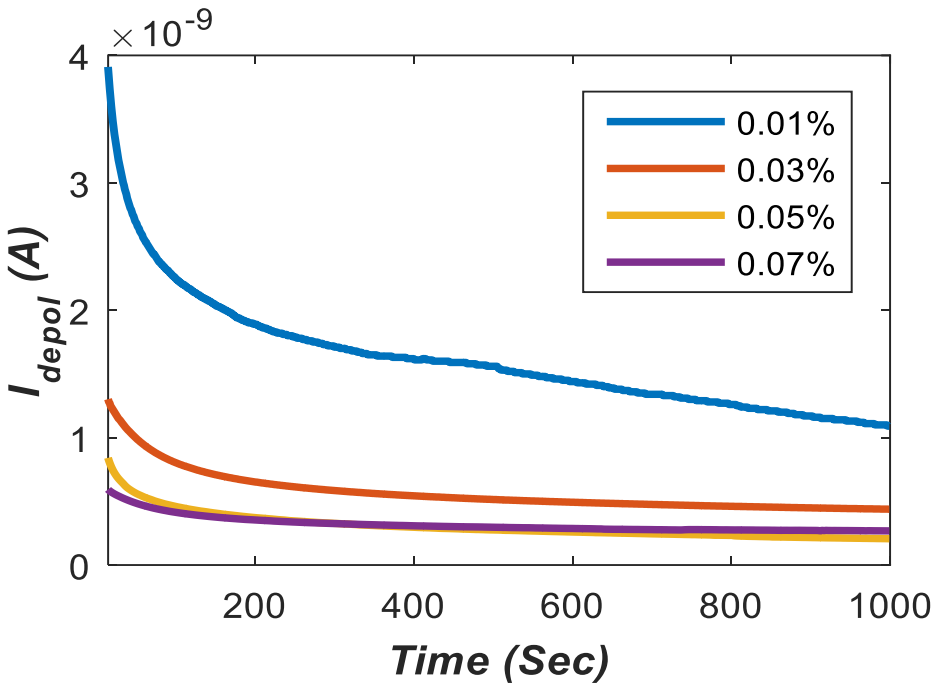

Fig. 5.3.1.4a. Variation of I_{dePol} at 24 hours by varying concentration

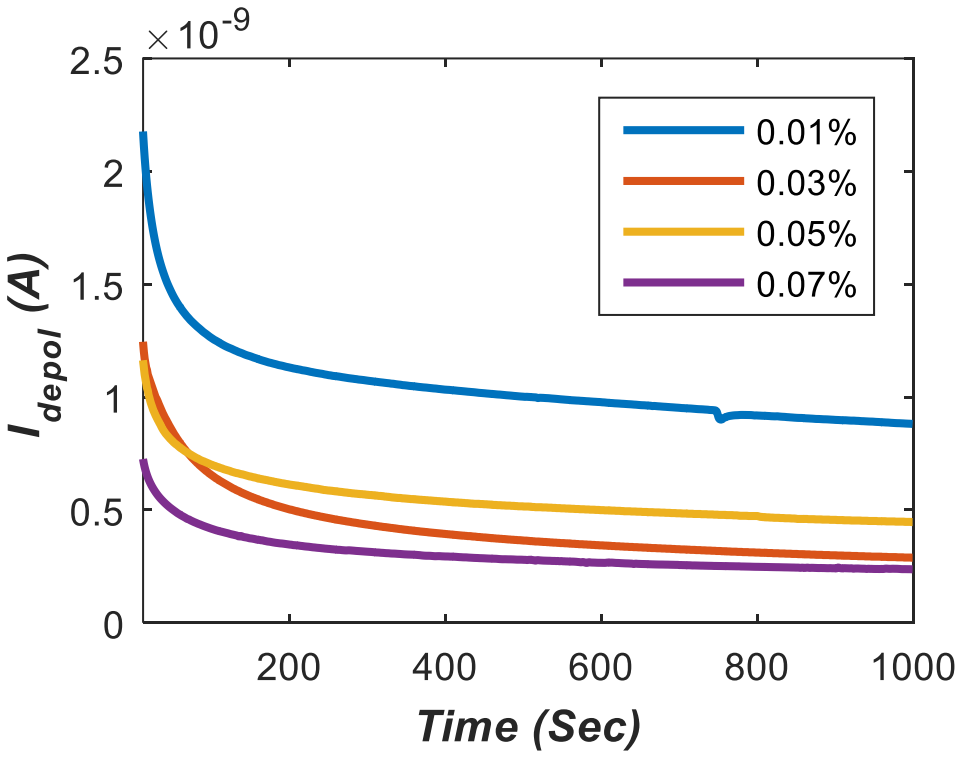

Fig.5.3.1.4b. Variation of I_{dePol} at 48 hours by varying concentration

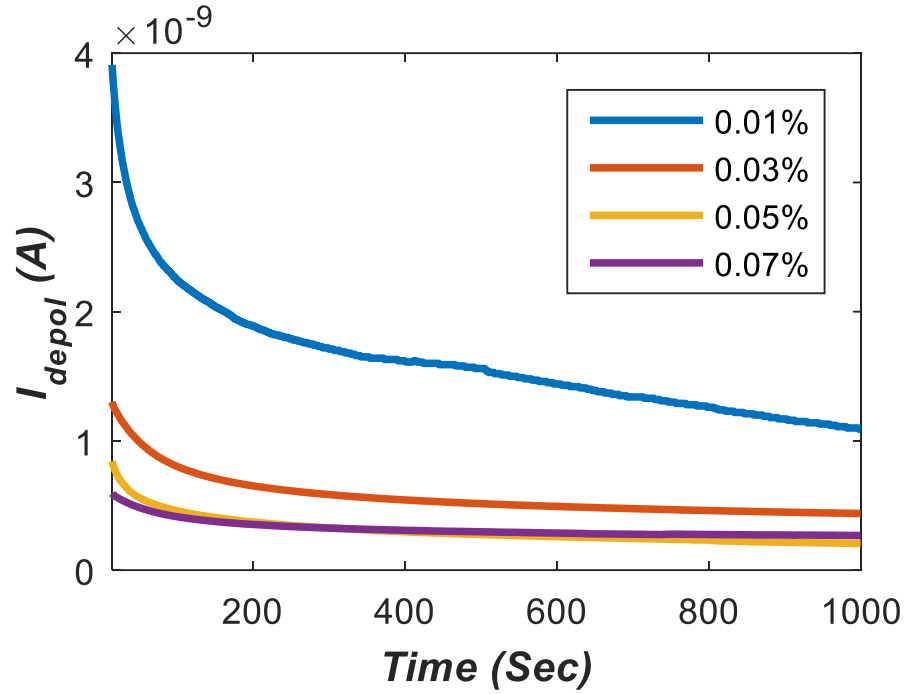

Fig. 5.3.1.4c. Variation of I_{dePol} at 72 hours by varying concentration

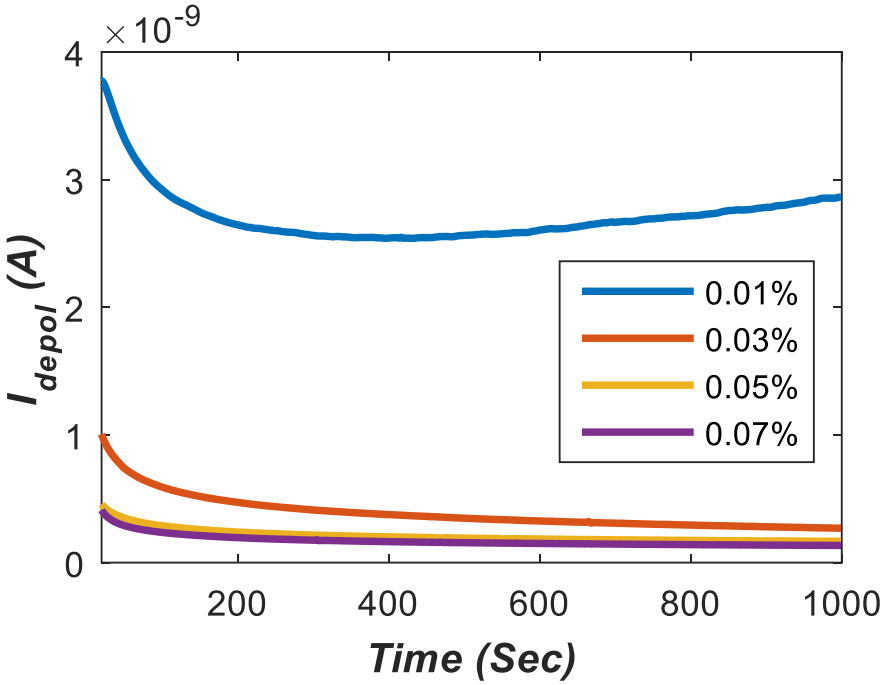

Fig.5.3.1.4d. Variation of I_{dePol} at 96 hours by varying concentration

5.3.1.5 Analysis of extended Debye model

In this section, the extended Debye model has been developed to state the insulation characteristics of the suggested model.

Using (3.13), the value of R_0 parameters of the extended Debye model for each nanofluid sample with different percentage concentrations of nanofluids at different hours from the instant of preparation has been shown in Table.5.3.

Table 5.3. R_0 parameters for each nanofluid sample

Percentage concentration	R_0 (24 hours) Ω	R_0 (48 hours) Ω	R_0 (72 hours) Ω	R_0 (96 hours) Ω
0.01%	4.4052e+08	7.7447e+08	7.8740e+08	5.645e+08
0.03%	3.2679e+09	3.1223e+09	3.4390e+09	4.059e+09
0.05%	2.1525e+08	2.0751e+08	2.3897e+08	5.325e+08
0.07%	3.1452e+08	3.5982e+08	4.1845e+08	6.9048e+8

In the following sections, variation of decaying coefficients and time constants obtained from the extended Debye model with variation of hours from the instant of preparation or percentage concentration of nanofluids has been discussed in detail.

5.3.1.5.1 Variation of decaying coefficient A_1 with several hours

The variation of decaying coefficient A_1 with several hours from the instant of preparation at different percentage concentrations (0.01%, 0.03%, 0.05% and 0.07%) of nanofluids has been shown in Fig.5.3.1.5.1a. Here, both the value that was recorded and the value derived from the suggested model have been taken into consideration for the A_1 parameter. Using curve fitting tool, fitting coefficients can be obtained using regression method with regression coefficient greater than 0.95 which point to good fitting. Here Table 5.4. represents fitted parameters of (5.1). In (5.1), hours and A_1 parameters have been denoted by $f(x)$and x, respectively.

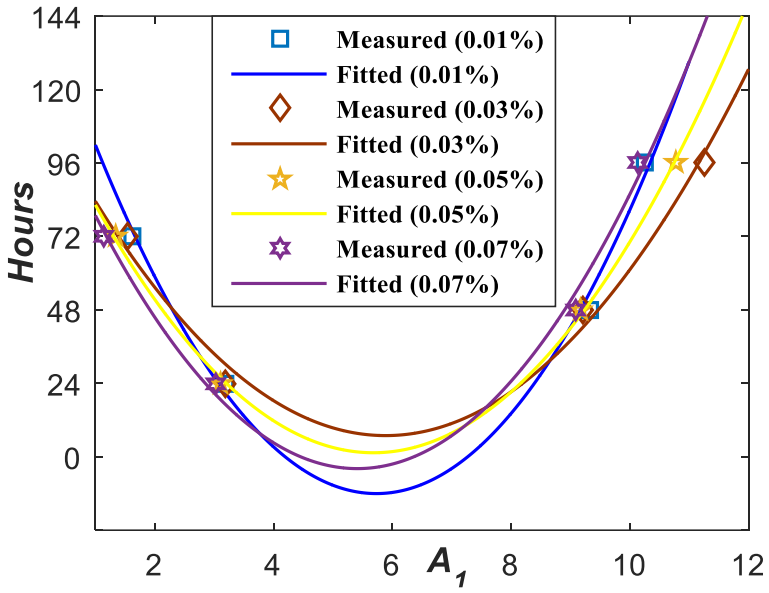

Fig.5.3.1.5.1a. Variation of A_1 parameter with several hours

$$f(x) = p_1x^2 + p_2x + p_3 \tag{5.1}$$

Table 5.4. Fitted parameters of (5.1)

	p_1	p_2	p_3	R^2	RMSE
(0.01% volume fraction)	3.964	0.6678	-0.4732	0.9776	0.3348
(0.03% volume fraction)	2.19	0.511	0.3106	0.9663	0.4104
(0.05% volume fraction)	3.226	0.5794	0.08073	0.9952	0.155
(0.07% volume fraction)	3.503	0.6907	-0.1273	0.9743	0.3587

5.3.1.5.2 Variation of decaying coefficient A_1 with different percentage concentration

The variation of decaying coefficient A_1 with different percentage concentration of the prepared nanofluid sample at four different hours from the instant of preparation has been shown in Fig.5.5.1.5.2. Using curve fitting tool, fitting coefficients can be obtained using regression method with regression coefficient more than 0.84 which point to good fitting. Here Table.5.5.

represents fitted parameters of (5.2). In (5.2), percentage concentration and A_1 parameters have been denoted by $f(x)$and x, respectively.

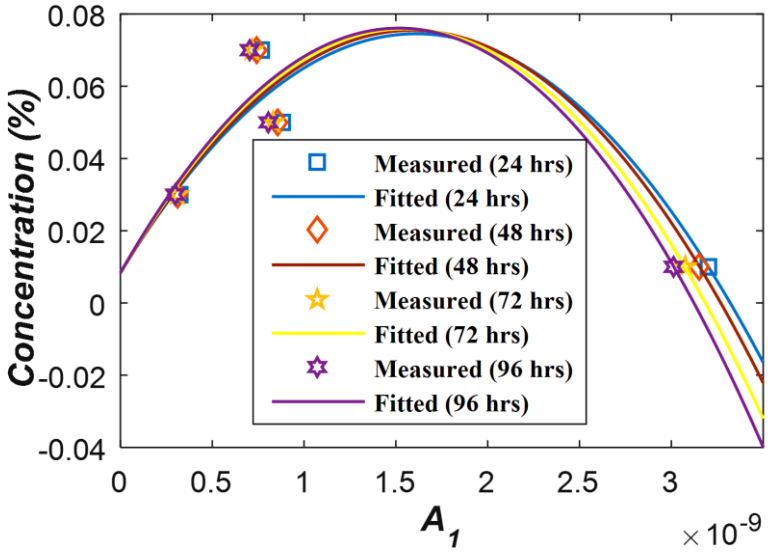

Fig.7.3.1.5.2a. Variation of A_1 parameter with different percentage concentration

$$f(x) = p_1x^2 + p_2x + p_3 \tag{5.2}$$

Table 5.5. Fitted parameters of (5.2)

	p_1	p_2	p_3	R^2	RMSE
(24 hours)	-0.0429	0.02073	0.07202	0.8451	0.0176
(48 hours)	-0.0437	0.02182	0.07277	0.845	0.01761
(72 hours)	-0.0441	0.02228	0.07308	0.8424	0.01776
(96 hours)	-0.04431	0.02248	0.07323	0.8457	0.01760

5.3.1.5.3 Variation of decaying coefficient A_2 with several hours

The variation of decaying coefficient A_2 with several hours from the instant of preparation at different percentage concentrations (0.01%, 0.03%, 0.05% and 0.07%) of nanofluids have been shown in Fig.5.3.1.5.3. Both the value that was recorded and the value derived from the suggested model have been taken into consideration for the A_2 parameter. Using curve fitting tool, fitting coefficients can be derived using regression method with regression coefficient more than 0.96 which point to good fitting. Here Table.5.6. represents fitted parameters of (5.3). In (5.3), hours and A_2 parameters have been denoted by $f(x)$and x, respectively.

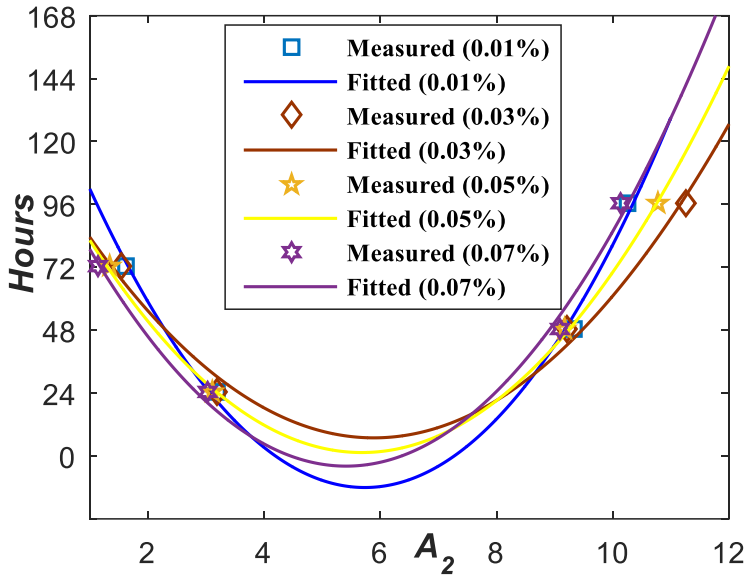

Fig.5.3.1.5.3a. Variation of A_2 parameter with several hours

$$f(x) = p_1x^2 + p_2x + p_3 \tag{5.3}$$

Table 5.6. Fitted parameters of (5.3)

A_2	p_1	p_2	p_3	R^2	RMSE
(0.01% volume fraction)	3.864	0.6678	0.0798	0.9745	0.3378
(0.03% volume fraction)	2.54	0.535	-0.4983	0.9663	0.4404
(0.05% volume fraction)	3.298	0.594	0.0901	0.9852	0.133
(0.07% volume fraction)	3.803	0.7107	-0.1713	0.9943	0.3598

5.3.1.5.4 Variation of decaying coefficient A_2 with different percentage concentration

The variation of decaying coefficient A_2 with different percentage concentration of the prepared nanofluid sample at four different hours from the instant of preparation has been shown in Fig.5.3.1.5.4a. Using curve fitting tool, fitting coefficients can be obtained using regression method with regression coefficient more than 0.84. Here Table.5.7. represents fitted parameters

of (5.4). In (5.4), percentage concentration and A_2 parameters have been denoted by *f(x)*and *x*, respectively.

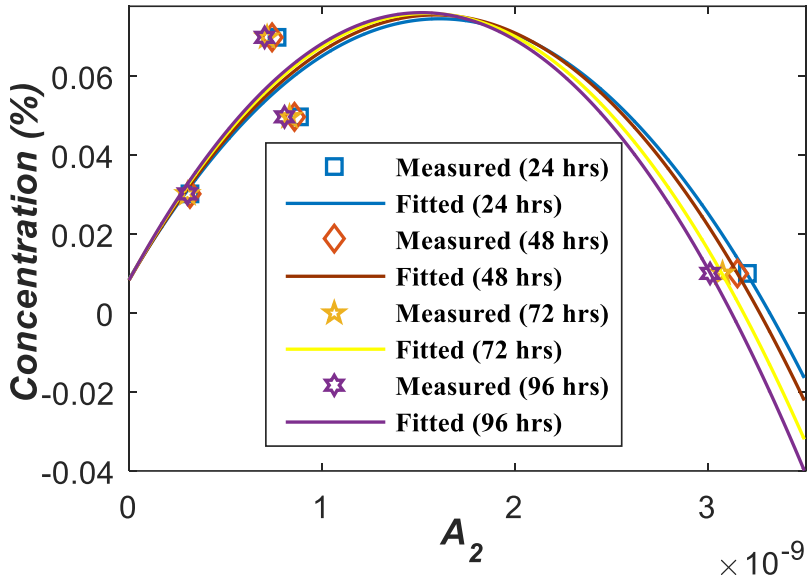

Fig.5.3.1.5.4a. Variation of A_2 parameter with different percentage concentration

$$f(x) = p_1x^2 + p_2x + p_3 \tag{5.4}$$

Table 5.7. Fitted parameters of (5.4)

A_2	p_1	p_2	p_3	R^2	RMSE
(24 hours)	-0.0443	0.02020	0.07304	0.8620	0.0175
(48 hours)	-0.0491	0.02142	0.07266	0.8535	0.01751
(72 hours)	-0.0414	0.02281	0.07318	0.8528	0.01576
(96 hours)	-0.0447	0.02235	0.07323	0.8667	0.01560

5.3.1.5.5 Variation of time constant τ_1 with several hours

The variation of time constant τ_1 with several hours from the instant of preparation at different percentage concentrations (0.01%, 0.03%, 0.05% and 0.07%) of nanofluids has been shown in Fig.5.3.1.5.5a. Both the value that was recorded and the value derived from the suggested model have been taken into consideration for the $\tau 1$ parameter. Here Table 5.8. represents fitted parameters of (5.5). In (5.5), hours and τ_1 parameters have been denoted by *f(x)*and x, respectively.

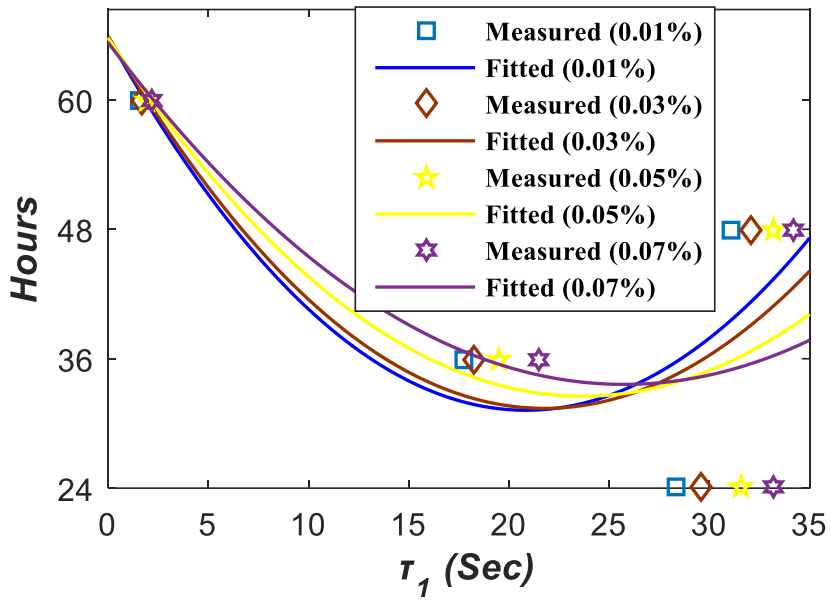

Fig.7.3.1.5.5a. Variation of τ_1 parameter with several hours

$$f(x) = p_1x^2 + p_2x + p_3 \tag{5.5}$$

Table 5.8. Fitted parameters of (5.5)

	p_1	p_2	p_3	R^2	RMSE
0.01% volume fraction)	1.186	-0.2029	1.611	0.6864	1.246
(0.03% volume fraction)	1.163	-0.2307	1.628	0.6793	1.226
(0.05% volume fraction)	1.023	-0.302	1.733	0.6426	1.337
(0.07% volume fraction)	0.883	-0.3565	1.833	0.6197	1.379

5.3.1.5.6 Variation of time constant (τ_1) with different percentage concentration

Fig.5.3.1.5.6a. depicts the variation of time constant τ_1 with different percentage concentration of the prepared nanofluid sample at four different hours from the instant of preparation. Here Table.5.9. represents fitted parameters of (5.6). In (5.6), percentage concentration and τ_1 parameters have been denoted by $f(x)$and x, respectively.

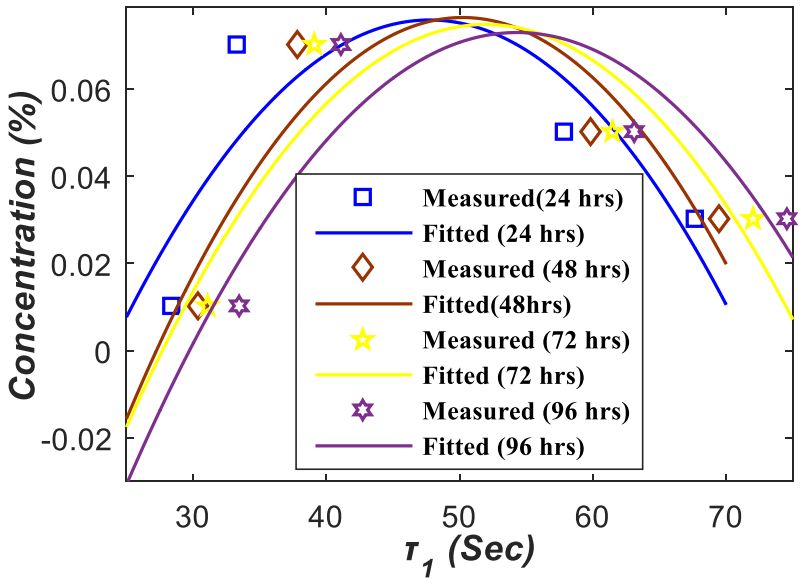

Fig.5.3.1.5.6a. Variation of τ_1 parameter with different percentage concentration

$$f(x) = p_1x^2 + p_2x + p_3 \tag{5.6}$$

Table 5.9. Fitted parameters of (5.6)

	p_1	p_2	p_3	R^2	RMSE
(24 hours)	-0.004759	0.005004	0.07569	0.5232	0.03088
(48 hours)	-0.04837	0.004616	0.07628	0.7125	0.024
(72 hours)	-0.04623	0.004877	0.07467	0.7144	0.0239
(96 hours)	-0.04369	0.005589	0.07277	0.6687	0.02247

5.3.1.5.7 Variation of time constant (τ_2) with several hours

The variation of time constant τ_2 with several hours from the instant of preparation at different percentage concentrations (0.01%, 0.03%, 0.05% and 0.07%) of nanofluids has been shown in Fig.5.3.1.5.7a. Both the value that was recorded and the value derived from the suggested model have been taken into consideration for the τ_2 parameter. Here Table.5.10. represents fitted parameters of (5.7). In (5.7), hours and τ_2 parameters have been denoted by $f(x)$and x, respectively.

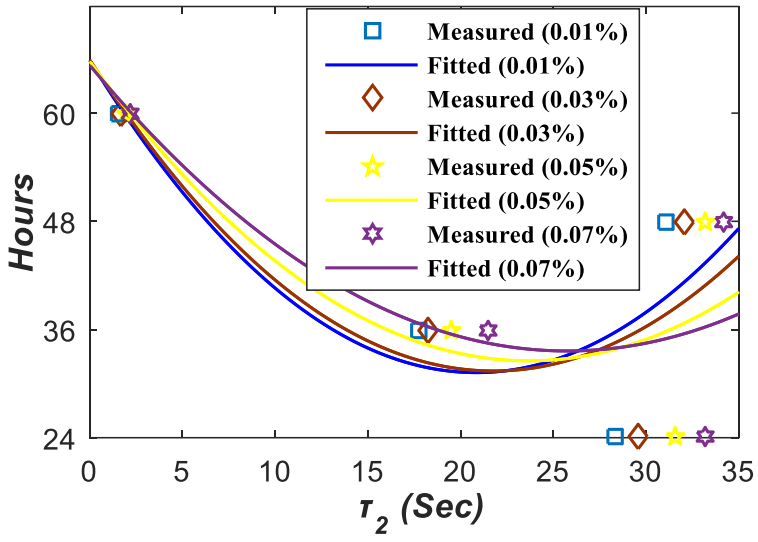

Fig.5.3.1.5.7a. Variation of τ_2 parameter with several hours

$$f(x) = p_1x^2 + p_2x + p_3 \tag{5.7}$$

Table 5.10. Fitted parameters of (5.7)

	p_1	p_2	p_3	R^2	RMSE
(0.01% volume fraction)	1.176	-0.2031	1.633	0.6879	1.256
(0.03% volume fraction)	1.193	-0.2402	1.648	0.6798	1.236
(0.05% volume fraction)	1.065	-0.312	1.753	0.6438	1.342
(0.07% volume fraction)	0.892	-0.3667	1.838	0.6206	1.389

5.3.1.5.8 Variation of time constant (τ_2) with different percentage concentration

The variation of time constant τ_2 with different percentage concentration of the prepared nanofluid sample at four different hours from the instant of preparation has been shown in Fig.5.3.1.5.8a. Both the value that was recorded and the value derived from the suggested model have been taken into consideration for the τ_2 parameter. Here Table.5.11. represents fitted parameters of (5.8). In (5.8), percentage concentration and τ_2 parameters have been denoted by *f(x)*and x, respectively.

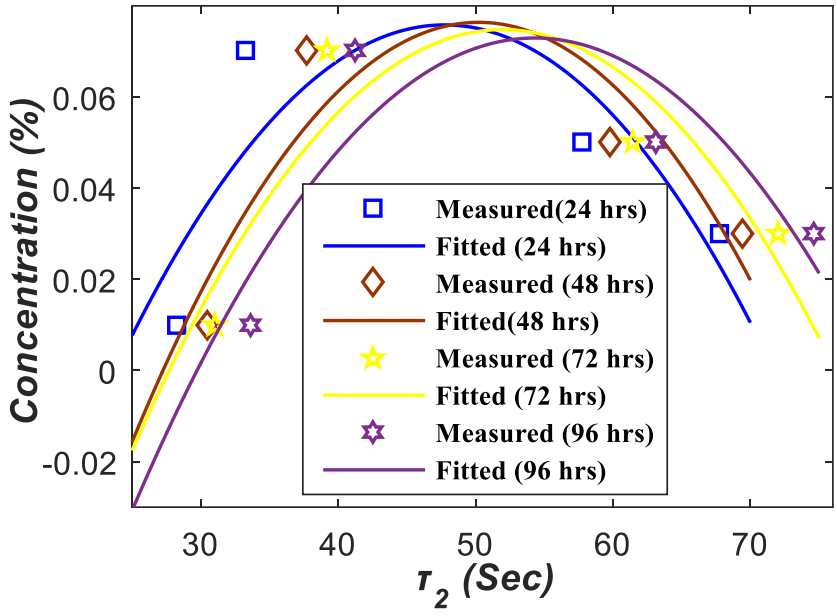

Fig.5.3.1.5.8a. Variation of τ_2 parameter with different percentage concentration

$$f(x) = p_1x^2 + p_2x + p_3 \tag{5.8}$$

Table 5.11. Fitted parameters of (5.8)

	p_1	p_2	p_3	R^2	RMSE
(24 hours)	-0.004775	0.005014	0.07601	0.5301	0.03093
(48 hours)	-0.04897	0.004658	0.07638	0.721	0.0243
(72 hours)	-0.04633	0.004881	0.07474	0.7208	0.0241
(96 hours)	-0.04373	0.005593	0.07299	0.6697	0.02265

5.3.1.5.9 Estimation of hours and percentage concentration using decaying coefficients and time constants

For predicting the hours from the instant of preparation and percentage concentration of the prepared ZnO nanofluids, eight empirical formulas have been established using the parameters obtained from extended Debye model as discussed in section 5.3.1.5.1-5.3.1.5.8. Now, to validate the aforementioned empirical expressions between hours from the instant of preparation or percentage concentration of nanofluids with decaying coefficients (A_1, A_2)) and time constants (τ_1, τ_2), two different samples (with 0.025% and 0.035% volume fraction of ZnO nanoparticles) have been prepared in the laboratory and the experiments have been conducted after 60 hours and 84 hours from the instant of preparation. After that, percentage errors have been calculated from the actual value and the predicted value of hours from the instant of preparation using (5.1, 5.3, 5.5 and 5.7) and has been presented in Table 5.12.

Table 5.12. Validation of (5.1), (5.3), (5.5), (5.7)

Parameters	Values	Parameters	Values
A_1(60 hours)	1.703e-09	τ_1 (60 hours)	9.802
A_1(84 hours)	9.378e-10	τ_1(84 hours)	4.184
A_2(60 hours)	1.6287e-09	τ_2 (60 hours)	10.02
A_2 (84 hours)	9.56e-10	τ_2 (84 hours)	6.12
hours using (7.9) for (60 hours)	59.744	hours using (7.13) for (60 hours)	59.940
hours using (7.9) for (84 hours)	83.568	hours using (7.13) for (84 hours)	83.941
hours using (7.11) for (60hours)	59.5836	hours using (7.15) for (60 hours)	58.88
hours using (7.11) for (84hours)	73.555	hours using (7.15) for (84 hours)	83.937
%error I	0.428%	%error I	0.0985%
% error II	0.5168%	%error II	0.0698%
% error III	0.6987%	%error III	1.09%
% error IV	1.42%	%error IV	0.075%

Similarly, percentage errors have been calculated from the actual value and the predicted value of percentage concentration of prepared nanofluid sample using (5.2, 5.4, 5.6 and 5.8) and has been presented in Table 5.13.

Table 5.13. Validation of (5.2), (5.4), (5.6), (5.8)

Parameters	Values	Parameters	Values
A_1(0.025%)	2.255e-10	τ_1 (0.025%)	9.802
A_1(0.035%)	3.287e-10	τ_1(0.035%)	4.184
A_2 (0.025%)	2.784e-10	τ_2 (0.025%)	10.02
A_2(0.035%)	3.497e-10	τ_2 (0.035%)	6.12
Percentage concentration using (7.10) for (0.025%)	0.02086	Percentage concentration using (7.14) for (0.025%)	0.02495
Percentage concentration using (7.10) for (0.035%)	0.034763	Percentage concentration using (7.14) for (0.035%)	0.0349
Percentage concentration using (7.12) for (0.025%)	0.02459	Percentage concentration using (7.16) for (0.025%)	0.0249
Percentage concentration using (7.12) for (0.035%)	0.03344	Percentage concentration using (7.16) for (0.035%)	0.031582
%error I	1.9812%	%error I	0.188%
% error II	0.6817%	%error II	0.2105%
% error III	3.054%	%error III	0.2974%
% error IV	4.65%	%error IV	1.0820%

5.3.2 Dielectric response in frequency domain

The dielectric characteristics of the laboratory-prepared mineral oil-based ZnO nanofluid samples in frequency domain were investigated through conducting frequency domain spectroscopy (FDS) measurements employing IDAX 300 for 0.01% concentration of nanofluids and DIRANA^{TM} for the rest of the samples at various percentage concentrations of nanofluids, respectively. In that analysis, the magnitude of voltage was fixed at 40Vrms.

From frequency domain spectroscopy measurements, some parameters are extracted (with hours and different percentage concentration), as shown in the following sections.

5.3.2.1 Variation of real component of the complex capacitance with several hours

Real component of the complex capacitance of different prepared samples has been plotted with several hours from the instant of preparation with four fixed concentration (0.01%, 0.03%, 0.05% and 0.07%), as shown in Fig. 7.3.2.1a - Fig. 7.3.2.1d. From Fig. 7.3.2.1a- Fig. 7.3.2.1d, it can be observed that the peak in the real component of complex capacitance occurs at low frequency and becomes minimal at high frequency. The real component of the complex capacitance is getting maximum at low frequencies due to space charge polarization. Because during space charge polarization, charge carriers near the surface of the electrodes reduces which in turn increases the capacitances but as a consequence, ac conductivity reduces.

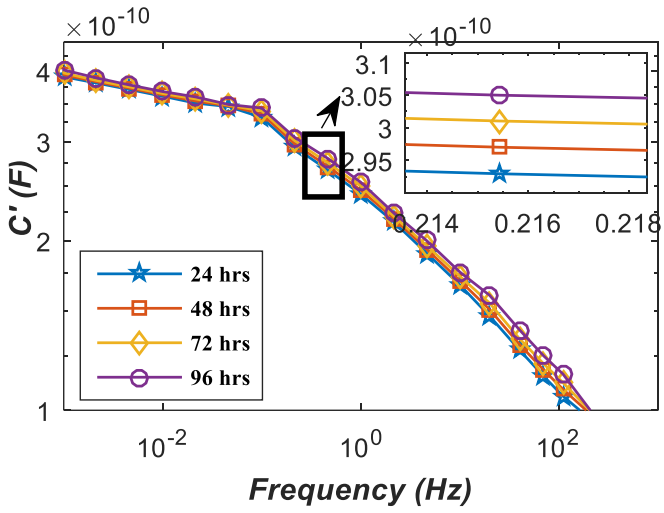

Fig.5.3.2.1a. Variation of C' with several hours at 0.01% Volume Fraction

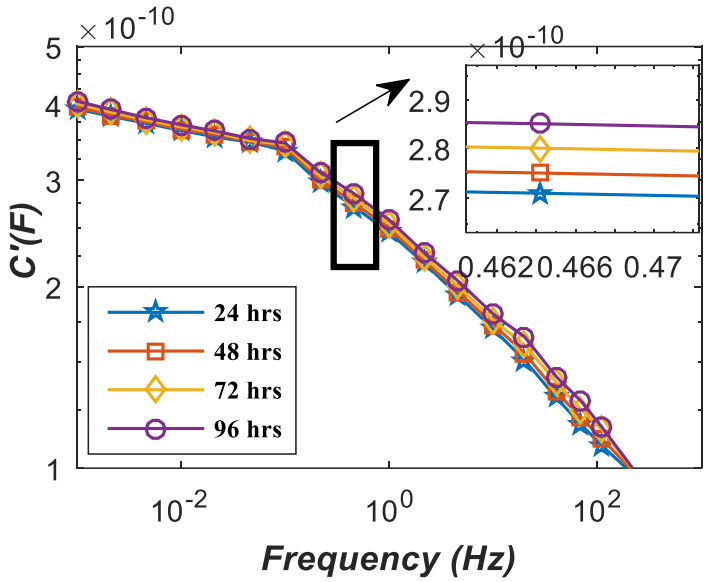

Fig. 5.3.2.1b. Variation of C' with several hours at 0.03% Volume Fraction

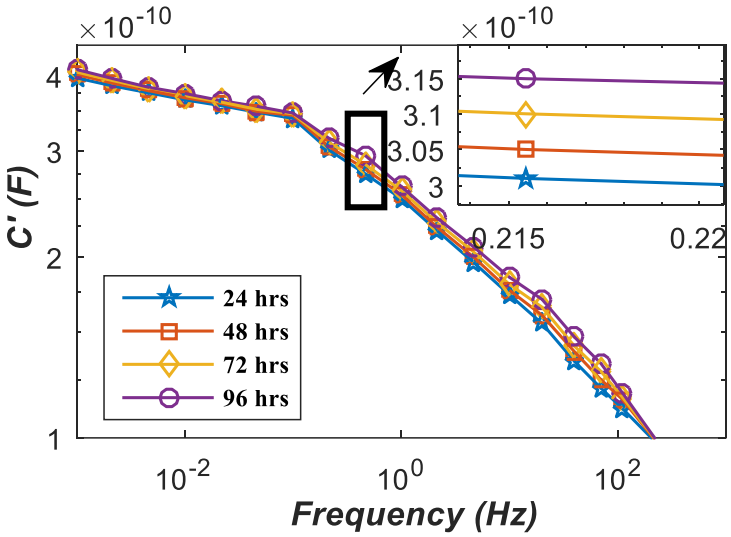

Fig.5.3.2.1c. Variation of C' with several hours at 0.05% Volume Fraction

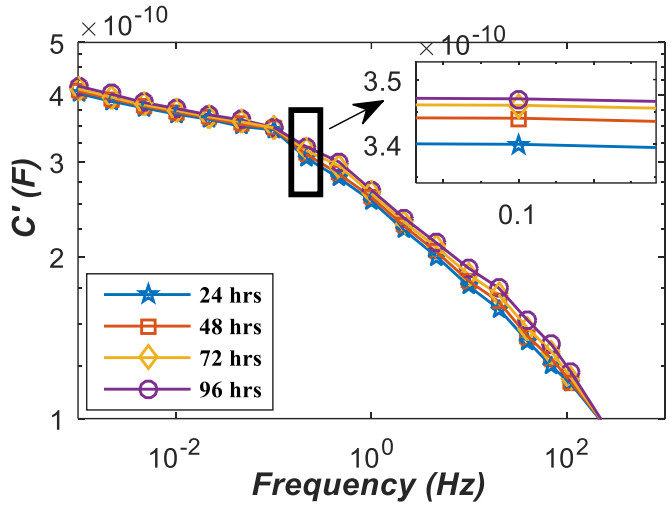

Fig. 5.3.2.1d. Variation of C' with several hours at 0.07% Volume Fraction

5.3.2.2a Variation of real component of the complex capacitance with different percentage concentration

The real component of the complex capacitance of the nanofluids has been plotted with various percentage concentration with four fixed hours from the instant of preparation as shown in Fig. 5.3.2.2a. -5.3.2.2d. From Fig.5.3.2.2a -5.3.2.2d, it can be observed that the real component of the complex capacitance value increases with increasing volume fraction of nanofluids, which means that, value of it is getting highest at 0.07% volume fraction compared to other percentage concentrations and getting lowest at 0.01% volume fraction of nanofluids.

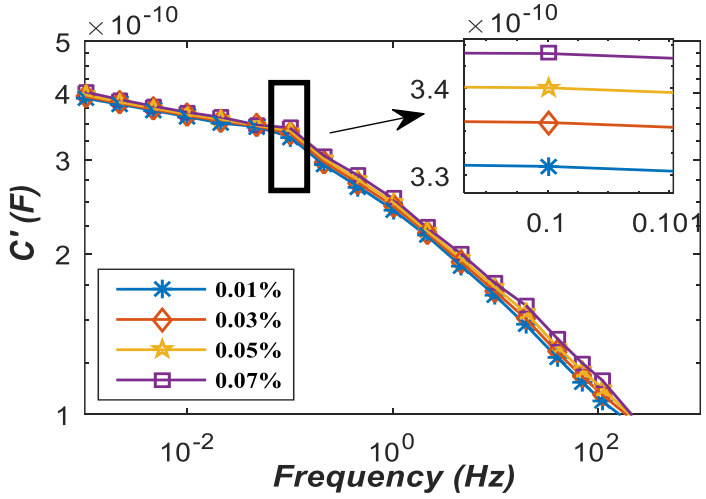

Fig.5.3.2.2a. Variation of C' at 24 hours by varying concentration

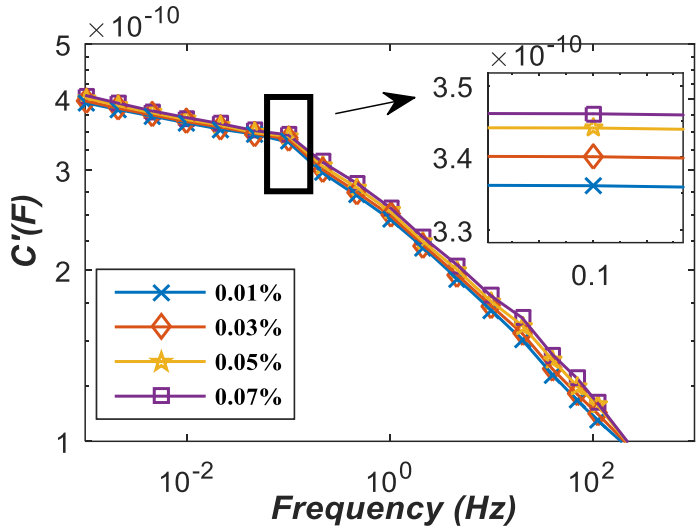

Fig. 5.3.2.2b. Variation of C' at 48 hours by varying concentration

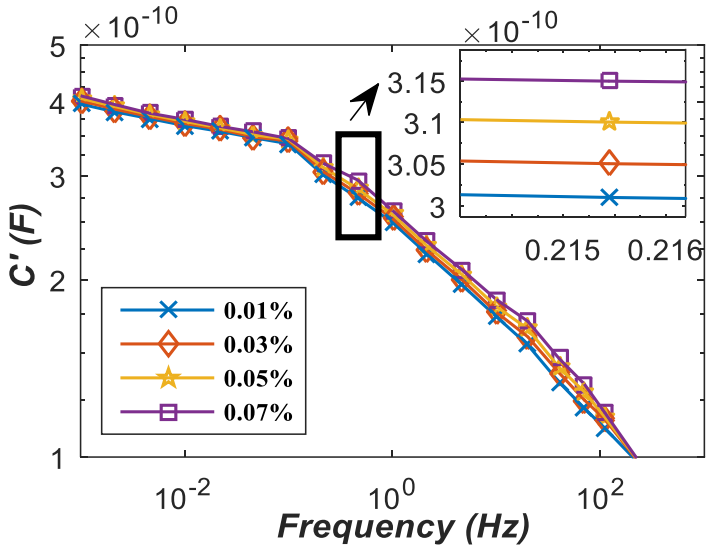

Fig. 5.3.2.2c. Variation of C' at 72 hours by varying concentration

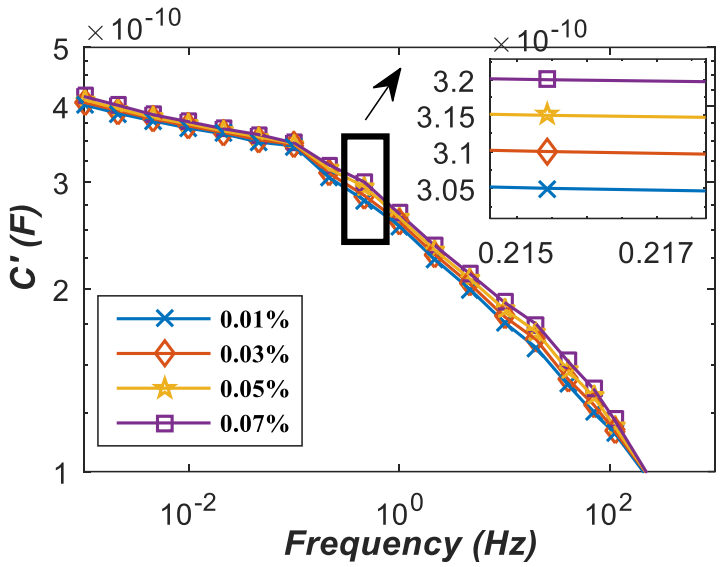

Fig.5.3.2.2d. Variation of $C^{'}$ at 96 hours by varying concentration

5.3.2.3 Variation of *tanδ* with several hours

In this section, the *tanδ* profiles of different prepared samples have been plotted with several hours from the instant of preparation at four fixed concentrations (0.01%, 0.03%, 0.05%, and 0.07%), which are shown in Fig. 5.3.2.3a - Fig. 5.3.2.3d. From Fig.5.3.2.3a -Fig5.3.2.3d, it can be observed that the peak in the tanδ profile occurs at low frequency and turns into a minimum at high frequency. It is because ion conduction and space charge polarization are both essential for mineral oil to behave as a dielectric. Positive and negative space charges are formed at the interfaces between various materials, such as between dielectric and conductor materials, when mobile positively and negatively charged particles are separated under an applied field.

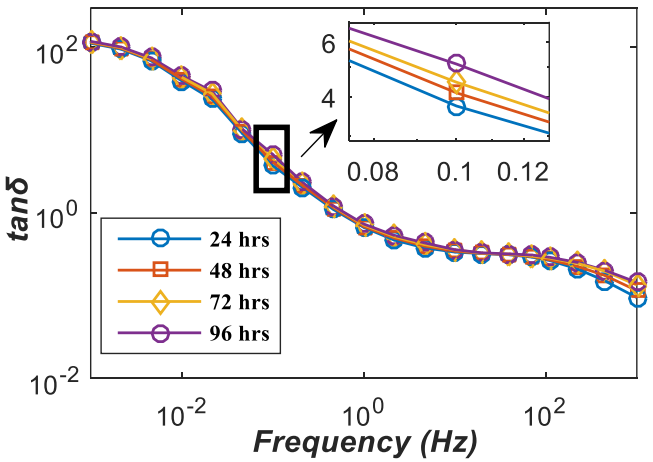

Fig.5.3.2.3a. Variation of tanδ with several hours at 0.01% volume fraction

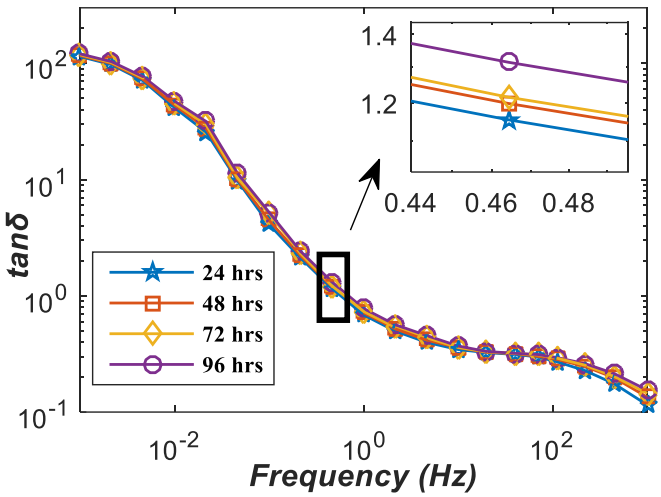

Fig. 5.3.2.3b. Variation of *tanδ* with several hours at 0.03% volume fraction

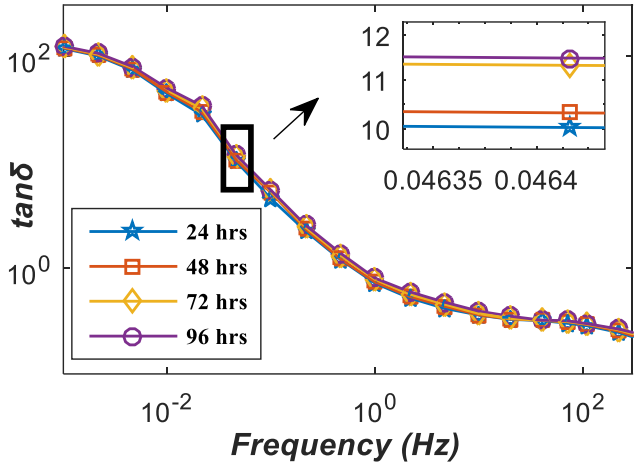

Fig.5.3.2.3c. Variation of *tanδ* with several hours at 0.05% volume fraction

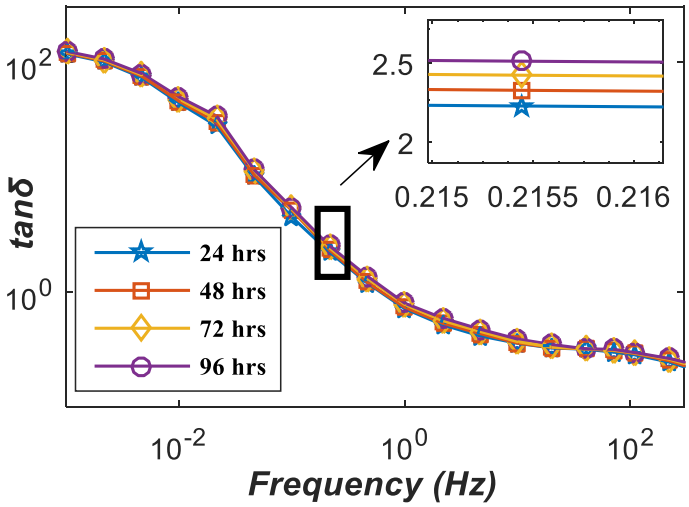

Fig. 5.3.2.3d. Variation of *tanδ* with several hours at 0.07% volume fraction

5.3.2.4 Variation of *tanδ* with different percentage concentration

The *tanδ* profiles of the nanofluids have been plotted with various percentage concentration with four fixed hours from the instant of preparation as shown in Fig. 5.3.2.4a. -5.3.2.4d. From Fig.5.3.2.4a -5.3.2.4d, it can be observed that the *tanδ* value increases with increasing volume fraction of nanofluids, which means the value of *tanδ* is getting highest at 0.07% volume fraction compared to other percentage concentrations.

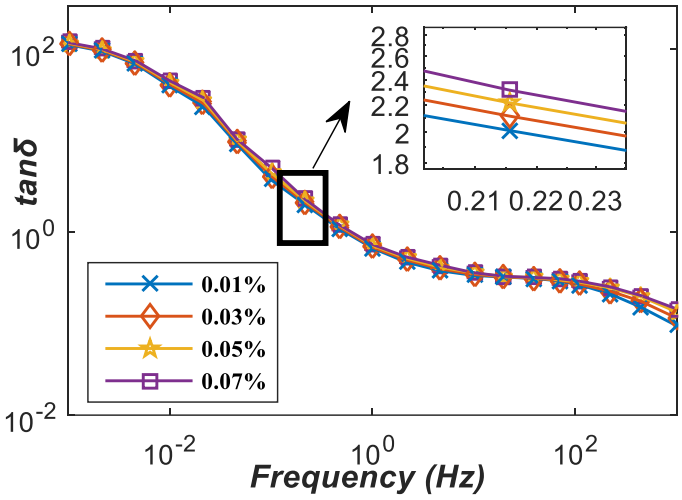

Fig. 5.3.2.4a. Variation of *tanδ* at 24 hours by varying Concentration

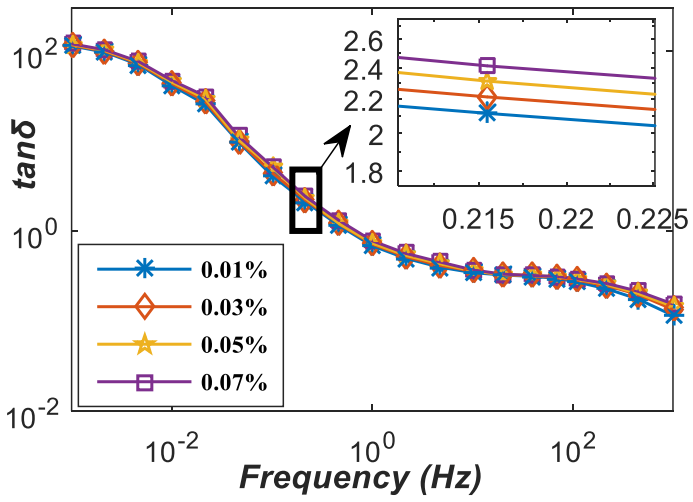

Fig. 5.3.2.4b. Variation of *tanδ* at 48 hours by varying Concentration

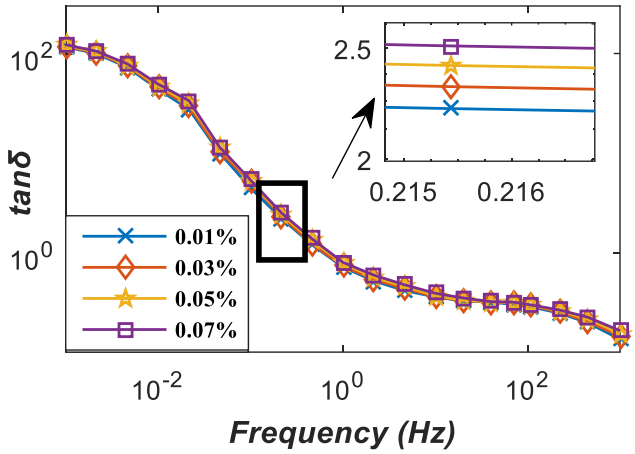

Fig. 5.3.2.4c. Variation of *tanδ* at 72 hours by varying Concentration

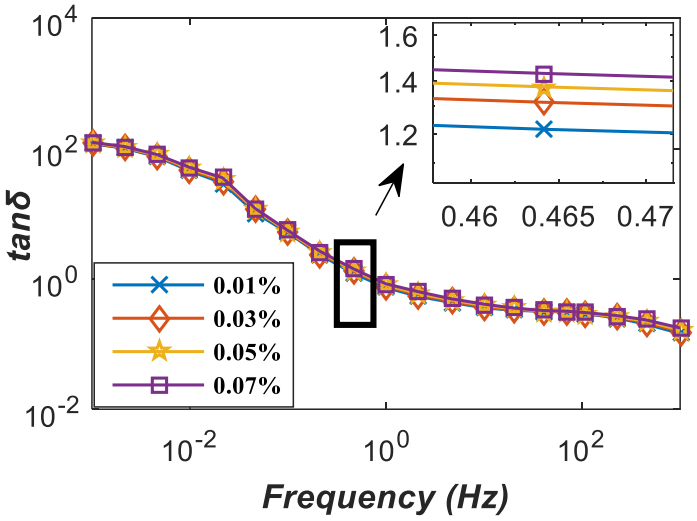

Fig. 5.3.2.4d. Variation of *tanδ* at 96 hours by varying Concentration

5.3.2.5 Variation of AC conductivity with several hours

AC conductivity of the mineral oil based ZnO nanofluids can be determined properly by using (3.20).

The variation of the ac conductivity of different prepared samples has been plotted with several hours from the instant of preparation at four fixed concentrations (0.01%, 0.03%, 0.05%, and 0.07%), as shown in Fig. 5.3.2.5a - Fig. 5.3.2.5d.

From Fig. 5.3.2.5a, it can be observed that the ac conductivity value is highest at 24 hours from the instant of preparation and become minimal at 48 hours. Similarly, from Fig.5.3.2.5b, it can be observed that the ac conductivity value gradually decreases from 48 hours to 96 hours from

the instant of preparation. Whereas, from Fig.5.3.5.c, it can observe that the ac conductivity value decreases from 48 hours to 72 hours from the instant of preparation. Again, from Fig.5.3.2.5d, it can be observed that the ac conductivity value increases at 24 hours from the instant of preparation and decreases at 72 hours.

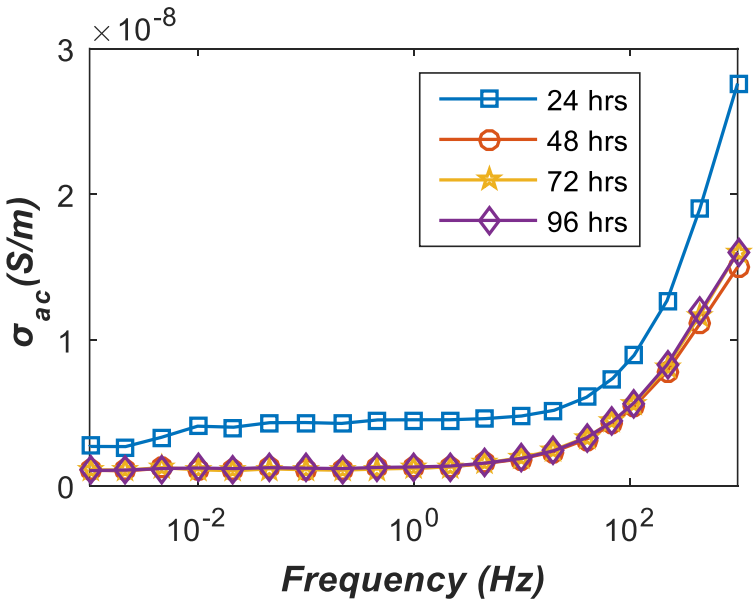

Fig.5.3.2.5a. Variation of σ_{ac} with several hours at 0.01% concentration

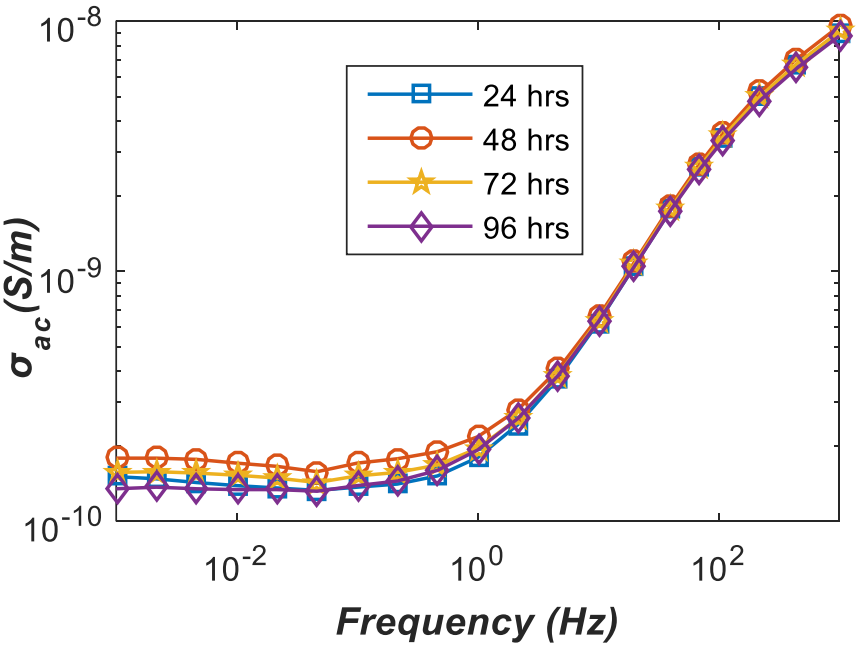

Fig. 5.3.2.5b. Variation of σ_{ac} with several hours at 0.03% concentration

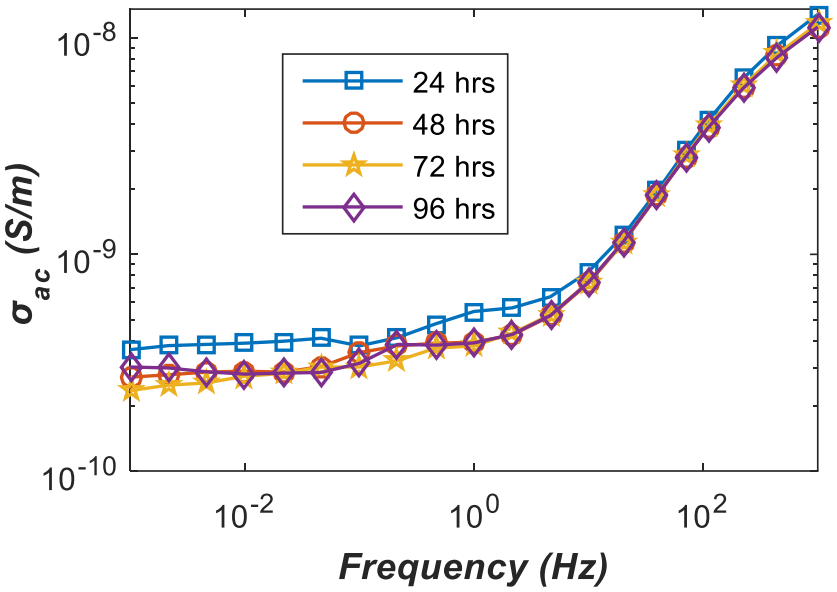

Fig. 5.3.2.5c. Variation of σ_{ac} with several hours at 0.05% concentration

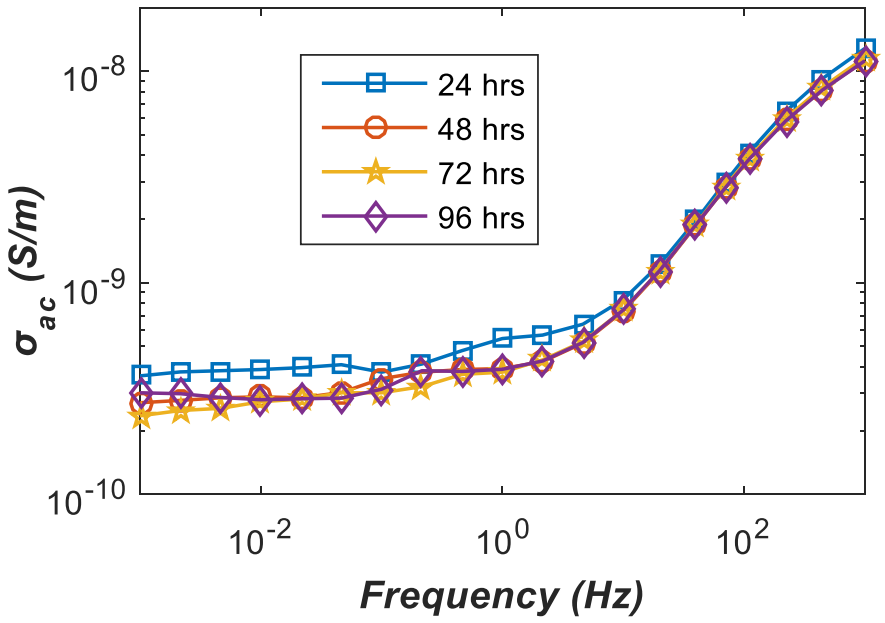

Fig. 5.3.2.5d. Variation of σ_{ac} with several hours at 0.07% concentration

5.3.2.6 Variation of AC conductivity with different percentage concentration

The ac conductivity of the nanofluid samples has been plotted with various percentage concentration with four fixed hours from the instant of preparation as shown in Fig. 5.3.2.6a. - 5.3.2.6d. From Fig.5.3.2.6a-5.3.2.6d it can be observed that the value of the ac conductivity is

highest at the 0.01% concentration of laboratory-prepared nanofluids and becomes minimal at the 0.03% concentration of nanofluids.

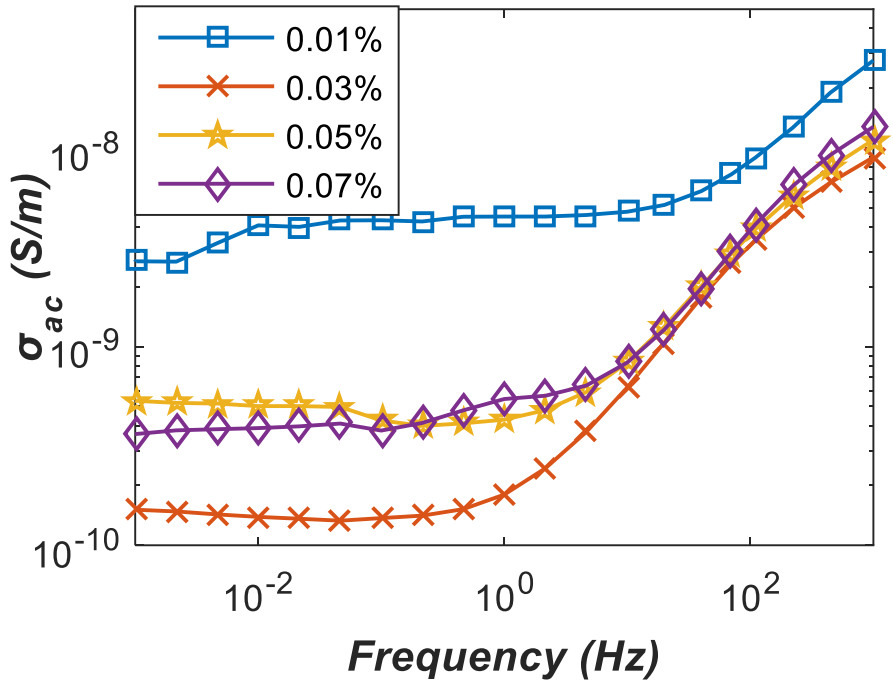

Fig. 5.3.2.6a. Variation of σ_{ac} at 24 hours by varying concentration

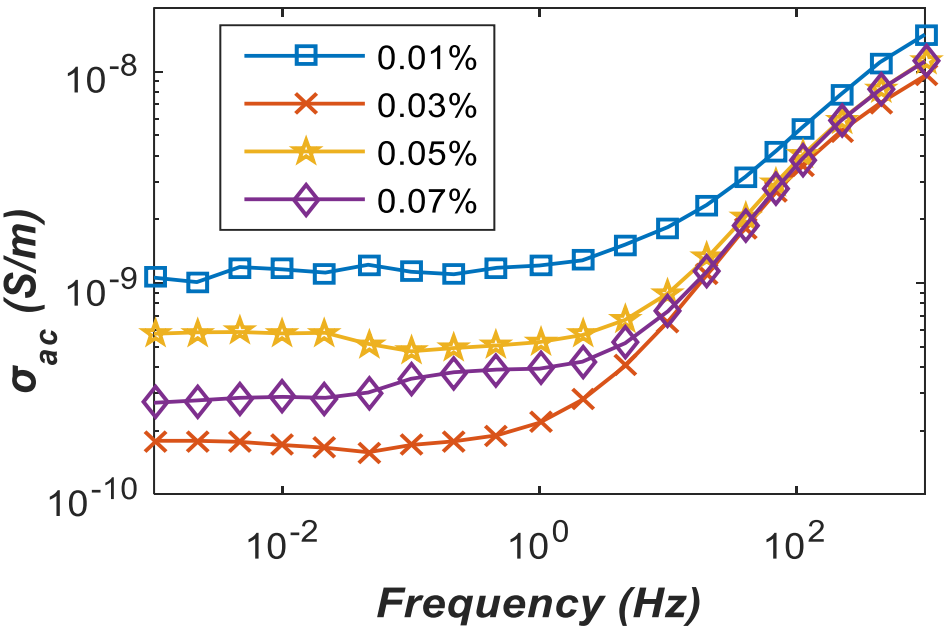

Fig. 5.3.2.6a. Variation of σ_{ac} at 48 hours by varying concentration

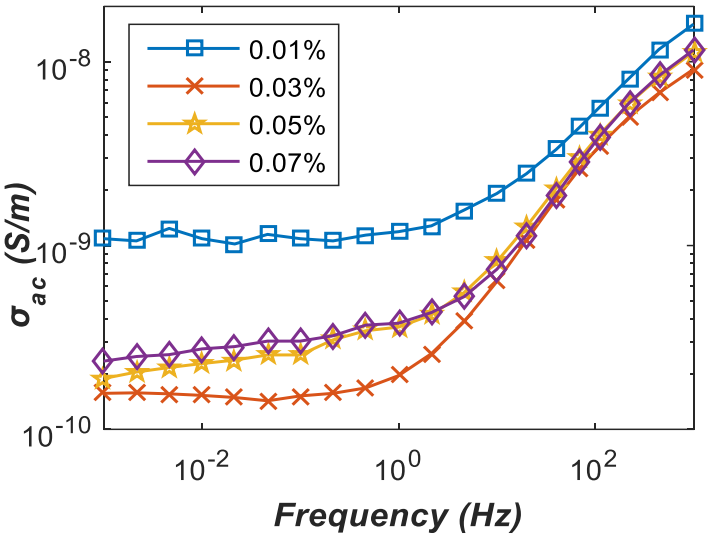

Fig.5.3.2.6c. Variation of σ_{ac} at 72 hours by varying concentration

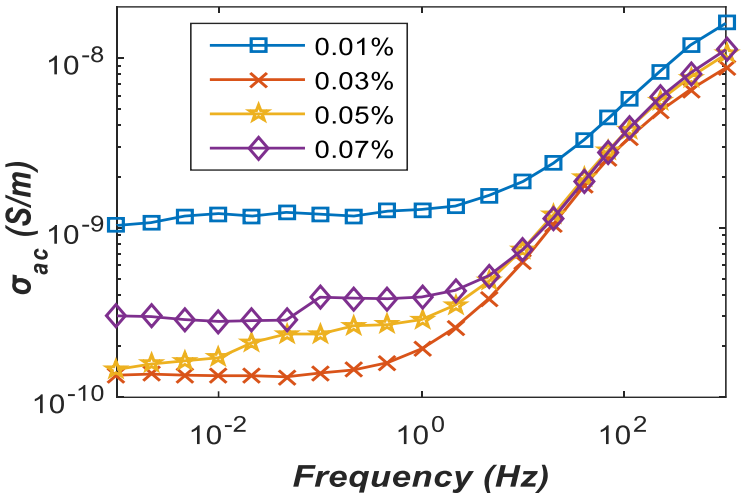

Fig. 5.3.2.6d. Variation of σ_{ac} at 96 hours by varying concentration

5.3.3 Study on low frequency dispersion of real and imaginary of complex capacitance and *tanδ* Profiles

From the aforementioned sections, it has been clearly observed that the peak in the dielectric loss factor occurs at low frequencies and reaches its minimum at high frequencies. From FDS, nature of *tanδ*, *C′* and *C″* at low frequency range (i.e. from 1mHz to 100Hz) can be easily analyzed. Therefore, a study of low frequency dispersion features of the real and imaginary components of the capacitance or tanδ has been realized to estimate hours and percentage concentration of the prepared nanofluid sample. In the following sections, change of *C′*, *C″* and *tanδ* with variation of hours from the instant of preparation or percentage concentration of nanofluids has been discussed in detail.

5.3.3.1 Change of real component of the complex capacitance with several hours curve.

The change of real component of the complex capacitance with several hours curve for the recorded value and value obtained from the suggested model at various concentrations of nanofluid samples has been shown in Fig.5.3.3.1a. Here Table. 5.14. represents fitted parameters of (5.9). which are obtained from the regression method using curve fitting tool. In (5.9), hours and ΔC′ have been denoted by *f(x)*and *x*, respectively.

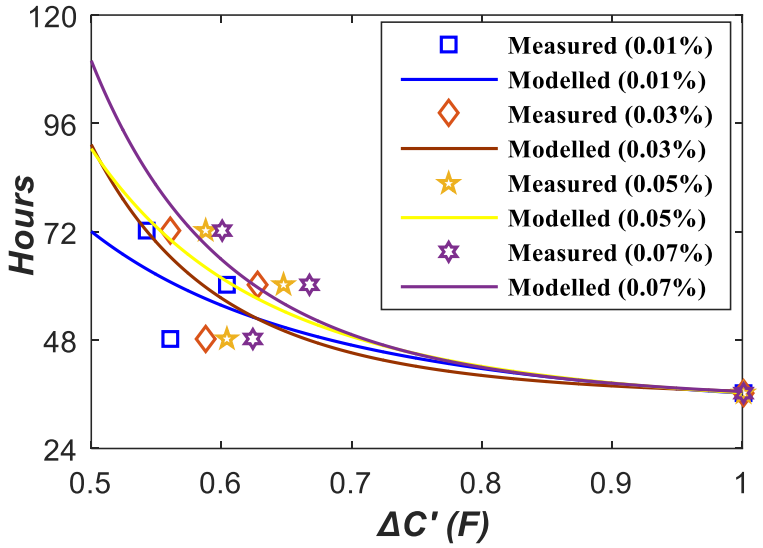

Fig.5.3.3.1a. $\Delta C'$ with several hours curve at different percentage concentration

$$f(x) = ax^b + c \tag{5.9}$$

Table 5. 14. Fitted Parameters of (5.9)

	A	b	c	R^2	RMSE
(0.01% Volume Fraction)	0.559	-2.664	0.4627	0.6357	1.35
(0.03% Volume Fraction)	0.137	-5.088	0.9191	0.6895	1.246
(0.05% Volume Fraction)	0.382	-3.678	0.6473	0.6452	1.332
(0.07% Volume Fraction)	0.2384	-4.734	0.8121	0.6722	1.28

5.3.3.2 Change of real component of the complex capacitance with different percentage concentration curve.

The change of real component of the complex capacitance with different percentage concentration curve for the recorded value and value obtained from the suggested model at different hours from the instant of preparation has been shown in 5.3.3.2a. Here Table 5.15. represents fitted parameters of (5.10) which are obtained from the regression method using curve fitting tool. In (5.10), percentage concentration and ΔC′ have been denoted by *f(x)*and *x*, respectively.

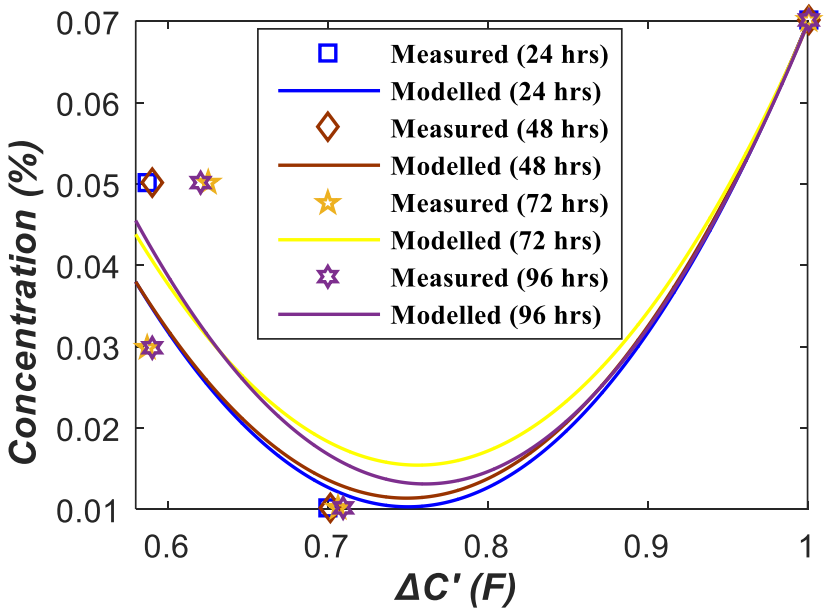

Fig.5.3.3.2a. ΔC with different percentage concentration curve at different hours

$$f(x) = p_1x^2 + p_2x + p_3 \tag{5.10}$$

Table 5.15. Fitted parameters of (5.10)

	p_1	p_2	p_3	R^2	RMSE
(Day 1)	-0.09576	0.07477	0.1118	0.9974	0.00132
(Day 2)	-0.02988	0.008353	0.06241	0.6753	0.02548
(Day 3)	-0.07034	0.04954	0.09275	0.8215	0.01889
(Day 4)	-0.0242	-0.04408	0.02185	0.643	0.02672

5.3.3.3 Change of imaginary component of the complex capacitance with several hours curve.

The change of imaginary component of the complex capacitance with several hours curve for the recorded value and value obtained from the suggested model at various concentrations of nanofluid samples has been shown in 5.3.3.3a. Using curve fitting tool, fitting coefficients have been derived through regression method with regression coefficient more than 0.95 which point to good fitting. Here Table 5.16. represents fitted parameters of (5.12). In (5.12), hours and ΔC″ have been denoted by *f(x)*and *x*, respectively.

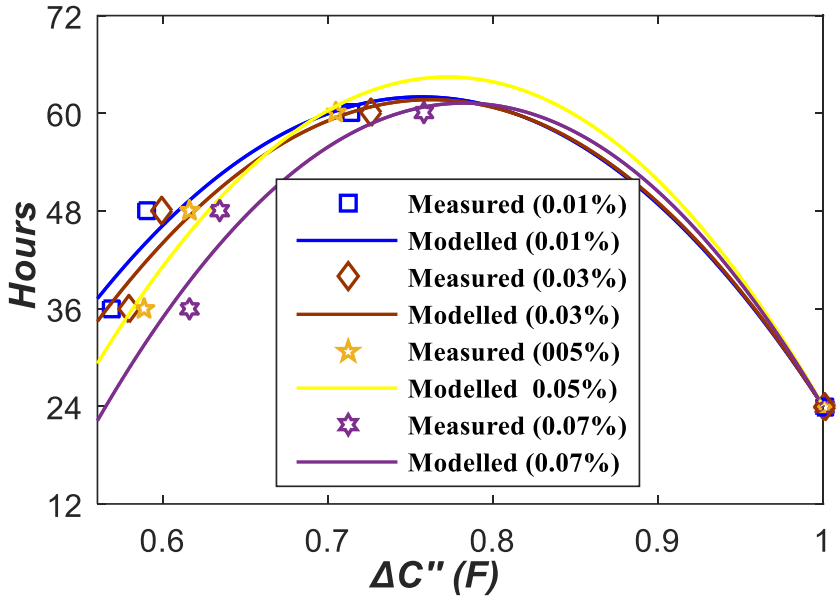

Fig.7.3.3.3a. $\Delta C''$ with several hours curve at different percentage concentration

$$f(x) = p_1x^2 + p_2x + p_3 \tag{5.11}$$

Table 5.16. Fitted Parameters of (5.11)

	p_1	p_2	p_3	R^2	RMSE
(0.01% Volume Fraction)	-54.05	81.96	-26.92	0.9923	0.1924
(0.03% Volume Fraction)	-54.67	83.32	-27.66	0.9927	0.1906
(0.05% Volume Fraction)	-57.55	88.43	-29.89	0.9919	0.2008
(0.07% Volume Fraction)	-57.67	88.84	-30.18	0.9983	0.09334

5.3.3.4 Change of imaginary component of the complex capacitance with different percentage concentration curve.

The change of imaginary component of the complex capacitance with different percentage concentration curve for the recorded value and value obtained from the prescribed model at different hours from the instant of preparation has been shown in Fig.5.3.3.4a. Using curve fitting tool, fitting coefficients have been derived using regression method with regression coefficient more than 0.95, which point to good fitting. Here Table. 5.17. represents fitted parameters of (5.12). In (5.12), percentage concentration and ΔC″ have been denoted by *f(x)*and *x*, respectively.

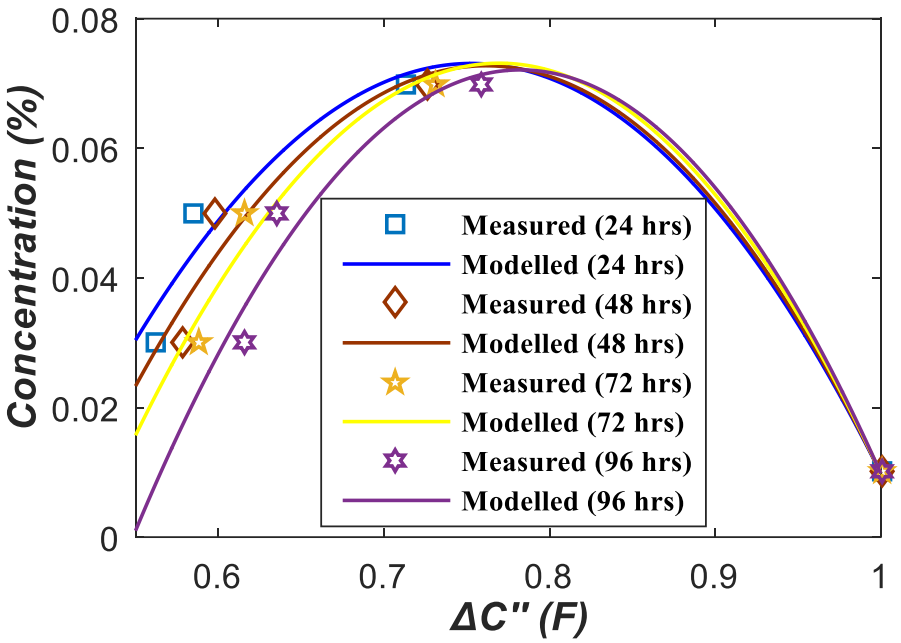

Fig.5.3.3.4a. $\Delta C''$ with different percentage concentration curve at different hours

$$f(x) = p_1x^2 + p_2x + p_3 \tag{5.12}$$

Table 5.17. Fitted Parameters of (7.12)

	p_1	p_2	p_3	R^2	RMSE
(24 hours)	-1.037	1.561	-0.5161	0.966	0.008262
(48 hours)	-1.105	1.683	-56.81	0.9593	0.009024
(72 hours)	-1.191	1.834	-0.6324	0.9792	0.006448
(96 hours)	-1.316	2.059	-0.7334	0.9612	0.00881

5.3.3.5 Change of *tanδ* with several hours curve.

The change of $tan\delta$ with several hours curve for the recorded value and value derived from the suggested model at different percentage concentrations of nanofluid samples has been shown in Fig.7.3.3.5a. Using curve fitting tool, fitting coefficients have been derived using regression method with regression coefficient more than 0.65. Here Table 5.18. represents fitted parameters of (5.13). In (5.13), hours and $\Delta tan\delta$ have been denoted by $f(x)$and x, respectively.

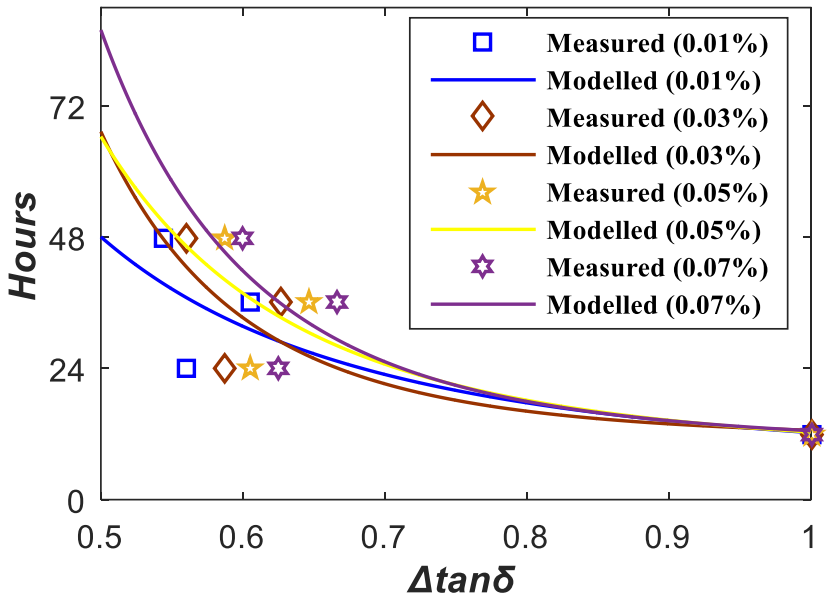

Fig.5.3.3.3a. Δ*tanδ* with several hours curve at different percentage concentration

$$f(x) = ax^b + c \tag{5.13}$$

Table 5.18. Fitted Parameters of (5.13)

	A	b	C	R^2	RMSE
(0.01% Volume Fraction)	0.03775	-7.04	1.019	0.7073	1.21
(0.03% Volume Fraction)	118.1	-1.322	0.7173	0.9287	0.5971
(0.05% Volume Fraction)	11.24	-0.4155	-1.954	0.8388	0.8979
(0.07% Volume Fraction)	-22.43	-1.079	4.094	0.6597	1.304

5.3.3.6 Change of *tanδ* with different percentage concentration curve.

The change of *tanδ* with different percentage concentration curve for the recorded value and value derived from the prescribed model at different hours from the instant of preparation is shown in Fig.5.3.3.6a. Using curve fitting tool, fitting coefficients have been derived using regression method with regression coefficient more than 0.95, which point to good fitting. Here Table. 5.19. represents fitted parameters of (5.14). In (5.14), percentage concentration and *Δtanδ* have been denoted by *f(x)*and *x*, respectively.

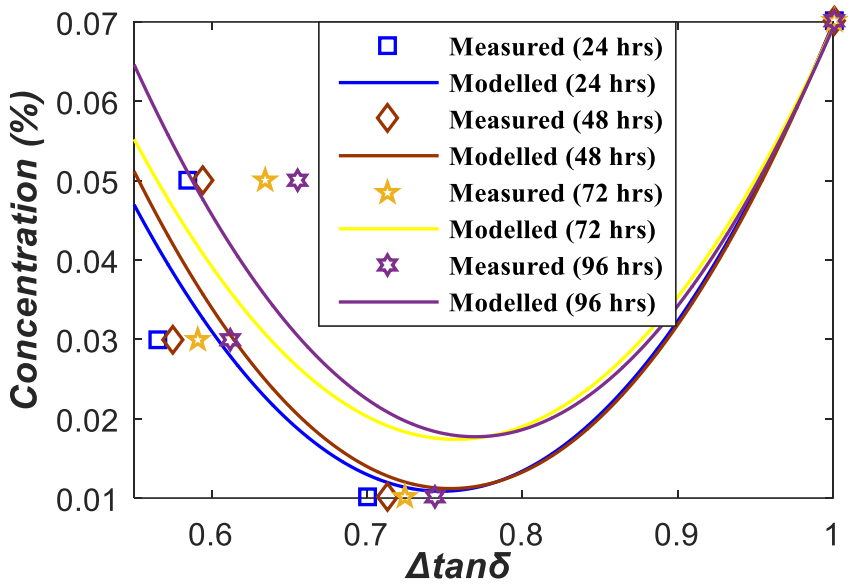

Fig.5.3.3.6a. Δ*tanδ* with different percentage concentration curve at different hours

$$f(x) = p_1x^2 + p_2x + p_3 \qquad (5.14)$$

Table 7.19. Fitted Parameters of (5.14)

	p_1	p_2	p_3	R^2	RMSE
(24 hours)	0.9245	-1.382	0.5276	0.8199	0.01898
(48 hours)	0.9643	-1.453	0.5589	0.8225	0.01884
(72 hours	0.8811	-1.334	0.5226	0.7099	0.02409
(96 hours)	0.9716	-1.496	0.5933	0.7074	0.02421

5.3.3.7 Estimation of hours and percentage concentration using LFD of real and imaginary component of the complex capacitance and *tanδ*

For predicting the hours from the instant of preparation and percentage concentration of the prepared ZnO nanofluids, six empirical formulas have been established using the parameters obtained from the LFD studies as discussed in section 5.3.3.1-5.3.3.6. Now, to validate the aforementioned empirical expressions between hours from the instant of preparation or percentage concentration of nanofluids using $\Delta C'$, $\Delta C''$ and $\Delta tan\delta$ with two different samples (with 0.025% and 0.035% volume fraction of ZnO nanoparticles) have been prepared in the laboratory and the experiments have been conducted after 60 hours and 84 hours from the instant of preparation. After that, percentage errors have been calculated from the actual value and the predicted value of hours from the instant of preparation using (5.9, 5.11, 5.13) and has been presented in Table 5.20.

Table 5.20. Validation of (5.9), (5.11), (5.13)

Parameters	**Values**	**Parameters**	**Values**	**Parameters**	**Values**
$\Delta C'$ (60 hours)	0.6147	$\Delta C''$ (60 hours)	0.5926	$\Delta tan\delta$ (60 hours)	0.6002
$\Delta C'$ (84 hours)	0.5608	$\Delta C''$(84 hours)	0.6595	$\Delta tan\delta$ (84 hours)	0.5561
hours using (7.21) for (60 hours)	59.698	hours using (7.23) for (60 hours)	58.4527	hours using (7.25) for (60 hours)	59.976
hours using (7.21) for (84 hours)	83.522	hours using (7.23) for (84 hours)	82.709	hours using (7.25) for (84 hours)	83.976
%error I	0.5210%	%error I	2.647%	%error I	0.03912%
% error II	0.5717%	%error II	1.56%	%error II	0.02836%

Similarly, percentage errors have been calculated from the actual value and the predicted value of percentage concentration of prepared nanofluid sample using (5.10, 5.12, 5.14) and has been presented in Table 5.21.

Table 5.21. Validation of (5.10), (5.12), (5.14)

Parameters	Values	Parameters	Values	Parameters	Values
$\Delta C'$ (0.025%)	0.6226	$\Delta C''$ (0.025%)	0.5585	$\Delta tan\delta$ (0.025%)	0.6322
$\Delta C'$ (0.035%)	0.5842	$\Delta C''$(0.035%)	0.5808	$\Delta tan\delta$ (0.035%)	0.5962
Percentage concentration using (7.22) for (0.025%)	0.0245	Percentage concentration using (7.24) for (0.035%)	0.02242	Percentage concentration using (7.26) for (0.025%)	0.0246
Percentage concentration using (7.22) for (0.035%)	0.0348	Percentage concentration using (7.24) for (0.035%)	0.0322	Percentage concentration using (7.26) for (0.035%)	0.03493
%error I	2.012%	%error I	11.46%	%error I	0.142%
% error II	0.5717%	%error II	8.65%	%error II	0.18726%

CHAPTER- 6

CONCLUSION

6.1 Conclusion

In this work, some advance methods have been discussed for the prediction of the time after the instant of sample preparation and the percentage concentration of nanofluids using dielectric spectroscopic methods. For these purposes, dielectric spectroscopic measurements have been conducted in both the time and frequency domains. From these measurements, several parameters have been extracted with variation of hours from the instant of preparation or with the variation of percentage concentrations of the laboratory prepared ZnO nanofluids. Therefore, a methodology has been developed through which hours from the instant of preparation or percentage concentration of the nanofluids can be predicted. Therefore, to validate numerous empirical equations which have been obtained through the aforementioned methodology, two samples have been prepared in the laboratory with two different percentage concentrations of nanofluids. After that, experiment has been conducted at two different instants from the time of preparation. Finally, percentage errors have been calculated using those measured values and calculated values. Based on these errors value, it has been stated that, the time after the instant of preparation and the percentage concentration of nanofluids have been predicted accurately. Hence, it can be concluded that, this study is helpful to prepare a long term stable nanofluids which may be used as a good alternative to mineral oil.

6.2 Future Scope

Future works can be directed in many different directions. Some of the possible works are mentioned below.

1. This work mainly studied the dielectric characteristics of mineral oil based nanofluids. In future, nanofluids will plan to prepare with biodegradable ester oils. Then, insulating characteristics of ester based nanofluids will be studied.
2. In future plan, it will be tried to investigate the aging characteristics of nanofluids of both mineral oil and vegetable oil.
3. In this study, some parameters have been identified to predict the stability of nanofluids. In future, it will be tried to establish the relation between these parameters and aging by-products.

REFERENCES

[1] P. Muangpratoom and N. Pattanadech, “Breakdown and Partial Discharge Characteristics of Mineral oil-based Nanofluids,” IET Science, Measurement and Technology, vol.12, no.5, pp.609-616, 2018

[2] N. Pattanadech, “Partial discharge inception voltage characteristics of mineral oil,” Ph.D. dissertation, Graz University of Technology, Graz, Austria, 2013.

[3] M.H. Ahmadi, A. Mirlohi, M.A. Nazari and R. Ghasempour, “A review of thermal conductivity of various nanofluids,” Journal of Molecular Liquids, vol.265, no.3, pp.181–188, 2018.

[4] I.Khan, K.saeed and I.khan, “Nanoparticles: properties, applications and toxicities -A review,” Arabian Journal of Chemistry, vol.12, no.2, pp.908-931, 2019.

[5] C. AJ, M. A. Salam, Q. M. Rahman, F. Wen, S. P. Ang, and W. Voon, ‘‘Causes of transformer failures and diagnostic methods—A review,’’ Renew. Sustain. Energy Rev., vol. 82, pp. 1442–1456,2018.

[6] M. I. Hasan, ‘‘Improving the cooling performance of electrical distribution transformer using transformer oil—Based MEPCM suspension,’’ Eng. Sci.Technol. Int. J., vol. 20, no. 2, pp. 502–510, 2017.

[7] M. J. Heathcote, ‘‘Electric power transformer engineering, third edition [book reviews],’’ IEEE Power Energy Mag., vol. 11, no. 5, pp. 94–95,2013.

[8] H. R. Sheppard, ‘‘A century of progress in electrical insulation 1886-1986,’’ IEEE Elect. Insul. Mag., vol. 2, no. 5, pp. 20–30, 1986.

[9] Choi, C., Yoo, H.S., Oh, J.M, “Preparation and heat transfer properties of nanoparticle-in-transformer oil dispersions as advanced energy-efficient coolants,” Curr. Appl. Phys., vol. 8, no.6, pp. 710–712,2008.

[10] S. Vishal and P. Vikas, ‘‘Transformer’s history and its insulating oil,’’ in Proc. 5th Nat. Conf. (INDIACom), Mar,2011.

[11] M. Rafiq et al., "The impacts of nanotechnology on the improvement of liquid insulation of transformers emerging trends and challenges," Journal of Molecular Liquids, vol.302, no.6, pp.112482, 2020.

[12] Primo, V.A., Garcia, B., Albarracin, R., "Improvement of transformer liquid insulation using nanodielectric fluids: a review," IEEE Electr. Insul. Mag., vol.34, no.3, pp. 13–26,2018.

[13] Wang, X., Tang, C., Huang, B., et al., "Review of research progress on the electrical properties and modification of mineral insulating oils used in power transformers," Energies, vol.11, no.3, pp. 487,2018.

[14] M. Rajnak et al., "Statistical analysis of AC dielectric breakdown in transformer oil-based magnetic nanofluids," Journal of Molecular Liquids, vol.309, no.3, pp.584-589, 2020.

[15] W.S. Zaengl, "Dielectric spectroscopy in time and frequency domain for HV power equipment. I. Theoretical considerations," IEEE Electr. Insul. Mag., vol.19, no.5, pp.5–19,2003.

[16] A. Ghaderi, A. Mingotti, F. Lama, L. Peretto and R. Tinarelli, "Effects of temperature on MV cable joints tan delta measurements," in Proceedings of IEEE Transactions on Dielectrics Instrument Measurement, vol.68, no.10, pp.3892–3898, 2019.

[17] A.K. Pradhan, C. Koley, B. Chatterjee and S. Chakravorti, "Determination of optimized slope of triangular excitation for condition assessment of oil-paper insulation by frequency domain spectroscopy," in Proceedings of IEEE Transaction on Dielectrics Electrical Insulation, vol.23, no.3, pp.1303–1312, 2016.

[18] S. Li, S. Yu, Y. Feng, "Progress in and prospects for electrical insulating materials', in Proc. IET High Volt., vol.1, no.3, pp. 122–129,2016.

[19] HC. Verma, A. Baral, S. Chakravorti, "Condition assessment of various regions within non-uniformly aged cellulosic insulation of power transformer using modified extended Debye model," IET Sci. Meas. Technol., vol.11, no.7, pp.939–947,2017.

[20] A. Kumar, H.C. Verma and A. Baral et al., "Estimation of paper-moisture in transformer insulation employing dielectric spectroscopy data," IET Sci. Meas. Technol., vol.12, no.4, pp. 536–54,2018.

[21] T. Rouse, "Mineral insulating oil in transformers," IEEE Electr. Insul. Mag., vol.14, no.3, pp. 6–16,1998.

[22] C. Claiborne, H. Pearce, “Transformer fluids,” IEEE Electr. Insul. Mag., vol. 5, no.4, pp. 16–19,1989.

[23] I. Fofana, “50 years in the development of insulating liquids,” IEEE Electr. Insul. Mag. vol.29, no.5, pp.13–25,2013.

[24] P. de Oliveira Fernandes, A.F. Balielo, H.M. Wilhelm, L.G. G. Feitosa and G.C. dos Santos, “Ageing performance of Brazilian paraffinic oil and naphthenic insulating oil,” in Proc. IEEE Electrical Insulation Conference (EIC), IEEE, pp. 360– 363,2017.

[25] X. Wang, C. Tang, B.o. Huang, J. Hao and G. Chen, “Review of research progress on the electrical properties and modification of mineral insulating oils used in power transformers,” Energies, vol.11, no.3, pp.487 ,2018.

[26] S.K. Das, S.U.S. Choi, W. Yu et al., “Nanofluids: science and technology,” (Wiley-Interscience, USA, 2008.

[27] M.E. Ibrahim, A.M. Abd-Elhady, M.A. Izzularab, “Effect of nanoparticles on transformer oil breakdown strength: experiment and theory,” IET Sci. Meas. Technol., vol.10, no.3, pp. 839–845,2016.

[28] Kakaç, Sadik; Anchasa, Pramuanjaroenkij, “Review of convective heat transfer enhancement with nanofluids,” International Journal of Heat and Mass Transfer., vol.52, no. (13–14), pp.3187–3196,2013.

[29] R. Saidur, K. Leong, H. Mohammad, “A review on applications and challenges of nanofluids,” Renew. Sust. Energy Rev., vol.15, no.3, pp. 1646–1668,2011.

[30] I. Fofana, “50 years in the development of insulating liquids,” IEEE Electr. Insul. Mag. vol.29, no.5, pp.13–25,2013.

[31] T. J. Lewis, “Nanometric dielectrics,” in Proc. IEEE Trans. Dielectr. Electr. Insul., vol. 1, no. 5, pp. 812–825, 1994.

[32] M. F. Frechette, M. L. Trudeau, H. D. Alamdari, and S. Boily, “Introduc-tory remarks on nanodielectrics,” in Proc.IEEE Trans. Dielectr. Electr. Insul., vol.11, no. 5, pp. 808–818, Oct. 2004.

[33] M. F. Frechette, “What are nanodielectrics?”, IEEE Electr. Insul. Mag., vol.29, no. 6, pp. 8–11, Nov. 2013.

[34] Y. Lv, Y. Zhou, C. Li, Q. Wang, and B. Qi, “Recent progress in nanofluids based on transformer oil: Preparation and electrical insulation properties,” IEEE Electr. Insul. Mag., vol. 30, no. 5, pp. 23–32, 2014.

[35] W. Sima, J. Shi, Q. Yang, S. Huang, and X. Cao, “Effects of conductivity and permittivity of nanoparticle on transformer oil insulation performance: Experiment and theory,” in Proc. IEEE Trans. Dielectr. Electr. Insul., vol. 22, no. 1, pp. 380–390, 2015.

[36] M. Rafiq, C. Li, Y. Ge, Y. Lv and K. Yi, “Effect of Fe_3O_4 Nanoparticle Concentrations on Dielectric Property of Transformer Oil,” in Proc. IEEE, 2016.

[37] Du, Y., Lv, Y., Li, C., et al., “Effect of semi conductive nanoparticles on insulating performances of transformer oil,” in Proc. IEEE Trans. Dielectr. Electr. Insul., vol.19, no.2 pp.770-776, 2012.

[38] M. Rafiq, C. Li, Y. Lv, K. Yi, S. Hussnain, “Preparation and Study of Breakdown Features of Transformer Oil Based Magnetic Nanofluids,” in Proc. IEEE, 2017.

[39] B. Chakraborty, S. Maur, A. K. Pradhan, B. Chatterjee and S. Dalai, “Study of Nonlinearity, Activation Energy, and Temperature Effect on Al2O3 and TiO2 Nanoparticle-Based Mixed Oil Characteristics by Dielectric Spectroscopy,” in Proc. IEEE Transactions on Dielectrics and Electrical Insulation, vol. 30, no. 3, pp. 997-1004, 2023,

[40] J. Zhang J. Du and B. Han et al., “Sonochemical formation of single-crystalline gold nanobelts,” Angew. Chem. Int. Ed., vol. 45, no.7, pp. 1116 – 1119 ,2006.

[41] R. Liu, L. Pettersson and A. Auletta et al., “Fundamental research on the application of nano dielectrics to transformers,” in Proceedings of Annual Report Conf. on Electrical Insulation and Dielectric Phenomena, pp. 423 – 427, Cancun, Mexico, 2011.

[42] P.P.C. Sartoratto, A.V.S. Neto and E.C.D. Lima et al., “Preparation and electrical properties of oil-based magnetic fluids,” J. Appl. Phys., vol.97, no.10, pp-917,2009.

[43] M. Chiesa, S.K. Das, “Experimental investigation of the dielectric and cooling performance of colloidal suspensions in insulating media,” Colloids Surf. A, Physicochem. Eng. Aspects, vol.335, pp. 88 – 97,2009.

[44] B. Du, X. Li, L.X and J.Li, “Thermal conductivity and dielectric characteristics of transformer oil filled with BN and Fe_3O_4 nanoparticles,” in Proc.IEEE Trans. Dielectr. Electr. Insul., vol.22, no.5, pp. 2530 – 2536, 2015.

[45] B. Du J. Li and F. Wang et al., "Influence of monodisperse Fe_3O_4 nanoparticle size on electrical properties of vegetable oil-based nanofluids," J. Nanometer., vol. 2015, pp. 3, 2015.

[46] Y. Lv, Y. Ge and Z. Sun et al., "Effect of nanoparticle morphology on pre-breakdown and breakdown properties of insulating oil-based nanofluids," Nanomaterials, vol. 8, no.7 pp. 476, 2018.

[47] V. Trisaksri and S. Wongwises, "Critical review of heat transfer characteristics of nanofluids," Renewable and Sustainable Energy Reviews, vol. 11, no. 3, pp. 512–523, 2007.

[48] X. Q. Wang and A. S. Mujumdar, "Heat transfer characteristics of nanofluids: a review," International Journal of Thermal Sciences, vol. 46, no. 1, pp. 1–19, 2007.

[49] X. Q. Wang and A. S. Mujumdar, "A review on nanofluids-part I: theoretical and numerical investigations," Brazilian Journal of Chemical Engineering, vol. 25, no. 4, pp. 613–630, 2008.

[50] Y. Li, J. Zhou, S. Tung, E. Schneider, and S. Xi, "A review on development of nanofluid preparation and characterization," Powder Technology, vol. 196, no. 2, pp. 89–101, 2009.

[51] S. Kakac and A. Pramuanjaroenkij, "Review of convective heat transfer enhancement with nanofluids," International Journal of Heat and Mass Transfer, vol. 52, no.13-14, pp. 3187–3196, 2009.

[52] K. Q. Ma and J. Liu, "Nano liquid-metal fluid as ultimate coolant," Physics Letters Section A, vol. 361, no. 3, pp. 252–256, 2007.

[53] G. Paul, M. Chopkar, I. Manna, and P. K. Das, "Techniques for measuring the thermal conductivity of nanofluids: a review," Renewable and Sustainable Energy Reviews, vol. 14, pp. 1913, 2010.

[54] H. Xie, W. Yu, and W. Chen, "MgO nanofluids: higher thermal conductivity and lower viscosity among ethylene glycol-based nanofluids containing oxide nanoparticles," Journal of Experimental Nanoscience, vol. 5, no. 5, pp. 463–472, 2010.

[55] I. Popa, G. Gillies and G. Papastavrou et al. "Attractive and repulsive electrostatic forces between positively charged latex particles in the presence of anionic linear polyelectrolytes," J. Phys. Chem. B, vol. 114, pp. 3170 – 3177, 2010.

[56] T. Missana, A. Adell, "On the Applicability of DLVO Theory to the Prediction of Clay Colloids Stability," J Colloid Interface Sci., vol. 230, no.8, pp.150-156,2000.

[57] Missana, T., Adell, A., "On the applicability of DLVO theory to the prediction of clay colloids stability" J. Colloid Interface Sci., vol.230, no. (1), pp. 150–156,2000.

[58] K. Bandara, C. Ekanayake and T.K. Saha, "Modelling the Dielectric Response Measurements of Transformer oil", in Proc.IEEE Transactions on Dielectrics and Electrical Insulation, vol. 22, no.2, pp.135-136,2015.

[59] S. Maur, B. Chakraborty, S. Dalai and B. Chatterjee, "Investigation on Effects of Thermal Ageing on LDPE Based on Polarization and Depolarization Currents", in Proc.IEEE International Conference for Convergence in Engineering, pp. 200-204,2020.

[60] J. Raha, N. Haldar and C. K Ghosh, "Intense orange emission from hydrothermally synthesized ZnO flower-like structure: effect of charge carrier—LO phonon interaction on emission characteristics", Springer-Verlag GmbH, DE part of Springer Nature 2021.